NASA-CR-197556

CAL-2260

National Aeronautics and Space Administration

HEA Gamma Ray Astronomy Research and Analysis Program

Annual Status Report for NAGW-2013

Submitted to:

Dr. Louis J. Kaluzienski
Astrophysics Division
Code SZC (GRA)
National Aeronautics and Space Administration
Washington, DC 20546

Submitted by:

The Trustees of Columbia University
in the City of New York
Box 20, Low Memorial Library
New York, New York 10027

Prepared by:

Columbia Astrophysics Laboratory
Departments of Astronomy and Physics
Columbia University
538 West 120^{th} Street
New York, New York 10027

Title of Research:

"A High Resolution Liquid Xenon Imaging Telescope for 0.3–10 MeV Gamma-Ray Astrophysics: Construction and Initial Balloon Flights"

Principal Investigator:

Prof. Elena Aprile
Columbia University

Report Period:

1 January 1994 – 31 December 1994

(NASA-CR-197556) A HIGH RESOLUTION LIQUID XENON IMAGING TELESCOPE FOR 0.3-10 MeV GAMMARAY ASTROPHYSICS: CONSTRUCTION AND INITIAL BALLOON FLIGHTS Annual Report, 1 Jan. - 31 Dec. 1994 (Columbia Univ.) 54 p

N95-17528

Unclas

G3/89 0034034

ANNUAL STATUS REPORT FOR NASA GRANT NAGW-2013

The project entitled "A High Resolution Liquid Xenon Imaging Telescope for 0.3-10 MeV Gamma-Ray Astrophysics: Construction and Initial Balloon Flights" was initiated with the submission in August 1992 of the proposal CAL-2015 in response to NASA Announcement of Opportunity NRA 92-OSSA-8.

For the second year of the project, covering the period 1 January 1994 through 31 December 1994 funds in the amount of $250,000 were allocated, under NASA Grant NAGW-2013.

The results achieved with a 10 liter LXe-TPC prototype during the second year can be summarized as follows:

- The charge response has been measured to be stable to within 0.1% for a period of time of about 100 hours.
- The electron lifetime has been measured to be in excess of 1 ms, corresponding to attenuation an length of the order of meters.
- The energy resolution has been measured to be consistent with previous results obtained with small volume chambers. At a drift field of 1 kV/cm the FWHM of 662 keV gamma-rays is 12% after corrections for electronic noise, shielding inefficiency and rise time effects. At 4 kV/cm the resolution improves to 7% FWHM.
- 3-D gamma-ray imaging has been demonstrated with a non-destructive orthogonal wires readout. A spatial resolution of order 1 mm has been achieved.
- Monte Carlo Simulation Results: expected background count rate at balloon altitude; background reduction algorithms; telescope's response to pointlike and diffuse sources.

The results obtained with the 10 liter LXe-TPC represent a significant progress towards the goal of construction and balloon-flight test of a LXe-Coded Aperture Telescope for MeV γ-ray astrophysics.

Most of the research work carried out during this second year of the project is summarized in the three articles attached as Appendix 1–3.

Appendix 1

DETERMINATION OF THE GALACTIC ^{26}AL SOURCE DISTRIBUTION WITH A NOVEL IMAGING TELESCOPE

E. APRILE
Physics Department and Columbia Astrophysics Laboratory
Columbia University
538 West 120th Street, New York, NY 10027

E.L. CHUPP
Physics Department and Institute for the Study of Earth,
Oceans, and Space
University of New Hampshire, Durham NH 03824

A. BOLOTNIKOV
NASA/Marshall Space Flight Center
Huntsville, AL 35812

P.P. DUNPHY
Physics Department and Institute for the Study of Earth,
Oceans, and Space
University of New Hampshire, Durham NH 03824

Submitted to: *The Astrophysical Journal*
1994 November 14

COLUMBIA UNIVERSITY

DEPARTMENTS OF

PHYSICS and ASTRONOMY

NEW YORK, NEW YORK 10027

Columbia Astrophysics Laboratory Contribution Number 557

DETERMINATION OF THE GALACTIC ^{26}AL SOURCE DISTRIBUTION WITH A NOVEL IMAGING TELESCOPE

E. APRILE
Physics Department and Columbia Astrophysics Laboratory
Columbia University
538 West 120th Street, New York, NY 10027

E.L. CHUPP
Physics Department and Institute for the Study of Earth,
Oceans, and Space
University of New Hampshire, Durham NH 03824

A. BOLOTNIKOV
NASA/Marshall Space Flight Center
Huntsville, AL 35812

P.P. DUNPHY
Physics Department and Institute for the Study of Earth,
Oceans, and Space
University of New Hampshire, Durham NH 03824

ABSTRACT

An instrument is described which will provide a direct image of γ-ray line or continuum sources in the energy range 300 keV to 10 MeV. We illustrate the use of this instrument to study the celestial distribution of the ^{26}Al isotope by observing the 1.809 MeV deexcitation γ-ray line. The source location accuracy is $2'$ or better. The imaging telescope is a liquid xenon time projection chamber coupled with a coded aperture mask (LXe-CAT). This instrument will confirm and extend the *COMPTEL* observations from the *Compton Gamma-Ray Observatory (CGRO)* with an improved capability for identifying the actual Galactic source or sources of ^{26}Al, which are currently not known with certainty. Sources currently under consideration include red giants on the asymptotic giant branch (AGB), novae, Type Ib or Type II supernovae, Wolf-Rayet stars, and cosmic-rays interacting in molecular clouds. The instrument could also identify a local source of the celestial 1.809 MeV γ-ray line, such as a recent nearby supernova.

Keywords: nucleosynthesis — γ-ray astronomy — imaging γ-ray telescope

1. INTRODUCTION

Observation of γ-ray lines from cosmic ray sources provides crucial information to enhance our understanding of the origin of the elements. Gamma-ray lines result from radioactive nuclei produced in stellar and cosmic ray nucleosynthetic processes as well as by direct nuclear excitation of stable nuclei. The first celestial radionuclide identified from its γ-ray emission was ^{26}Al (1.03 Myr meanlife) which decays by positron emission or electron capture to ^{26}Mg giving a line at 1.809 MeV. Following the independent predictions of Arnett (1977) and Ramaty and Lingenfelter (1977), this line was observed by the high energy resolution spectrometer on the *HEAO 3* satellite (Mahoney et al. 1984), and was subsequently confirmed by the *SMM* γ-ray spectrometer (Share et al. 1985). Since these satellites detected the largest flux from the direction of the Galactic center ($\sim 5 \times 10^{-4}$ photons cm^{-2} s^{-1} rad^{-1}), it was tacitly assumed that the putative sources of ^{26}Al are at a typical Galactic center distance of $\sim$ 8.5 kpc. This would imply that $\sim 3 - 4$ M$_\odot$ of ^{26}Al currently resides in the interstellar medium (ISM). Additional observations of the ^{26}Al γ-ray line made with several balloon borne instruments (von Ballmoos, Diehl, and Schönfelder 1987; MacCallum et al. 1987; Varendorff and Schönfelder 1991; Teegarden et al. 1991; Malet et al. 1991), confirmed its intensity in the direction of the Galactic center. The instruments used for all these observations were telescopes with wide fields-of-view (FOV) and poor angular resolution.

The *COMPTEL* and OSSE instruments on the *Compton Gamma Ray Observatory (CGRO)* are continuing detailed imaging observations of the spatial distribution of the ^{26}Al γ-ray emission with greatly improved sensitivity and angular resolution. The ongoing *COMPTEL* observations have been described in a succession of papers by Diehl et al. (1993a, b, c, d; 1994a, b, c). The *COMPTEL* 1.809 MeV images, currently available for the Galactic plane, reveal broadly peaked emission roughly compatible with the molecular (CO) gas distribution, but clumpy emission patches are evident at other Galactic longitudes (e.g., Diehl et al. 1994b, c). The central emission, while apparently nonuniform, appears to extend over a Galactic longitude range $-35° < \ell < 40°$ but the maximum is not at the Galactic center. The integrated flux from this inner region of the Galaxy is 1.9×10^{-4} photons cm^{-2} s^{-1}. Emission enhancements have also been reported from an extended region ($\sim 10°$ across) in the direction of Vela ($\ell = 263°$) and toward the Eta Carina galactic arm (ℓ=285°). The total flux reported for the Vela feature is 2.2×10^{-5} photons cm^{-2} s^{-1}. In the case of emission from the Vela region, two plausible sources (Oberlack et al. 1994) are the supernova remnant ($\ell = 263.9°$, b= -3.3°) and the Wolf-Rayet binary WR II ($\ell = 262.8°$, b = -7.7°). It is clear from these observations that our current knowledge of the distribution of ^{26}Al is dramatically different from that based on the earlier (pre-*COMPTEL*) satellite and balloon observations. Basically it was then believed that quasi continuous spatial γ-ray emission would reflect the smeared locations of explosive nucleosynthetic events over the past million years in the central part of the Galaxy. Now there is a distinct possibility that the required amount of ^{26}Al could be well below the few M$_\odot$ needed for sources at the Galactic center distance if it should be confirmed that several relatively close sources such as the (unconfirmed) Vela remnant at a distance less than 500 pc contribute. In fact, Diehl et al. (1994c) now estimate that the total Galactic mass of ^{26}Al is <1 M$_\odot$!

Further advances in our understanding of the origin of the ^{26}Al requires instruments with higher angular resolution and greater flux sensitivity. Ultimately, instruments capable of high energy resolution measurements will be needed to study the profile of the intrinsically narrow line which could reveal the temperature and motion of the emitting regions (Ramaty and Lingenfelter 1977).

In this paper we first review, briefly, the candidate sources for the ^{26}Al and the current γ-ray observations obtained by *COMPTEL* (§2). We then present the new imaging telescope (§3.1), with a special emphasis on the application of a liquid xenon ionization chamber as three-dimensional

(3-D) γ-ray imager and calorimeter (§3.2), followed by a short summary of recent experimental results obtained with a 10 liter liquid xenon prototype detector (§3.3). Monte Carlo simulations are presented in §4 to demonstrate the imaging response of the instrument both as balloon- and satellite-borne instrument. The instrument's capabilities will be confirmed by observations of the Crab Nebula in a planned balloon borne experiment.

2. SOURCES OF ^{26}AL PRODUCTION

Whatever the site of production of ^{26}Al, the basic nucleosynthetic process involved is ^{25}Mg(p,γ) ^{26}Al with the seed nuclide ^{25}Mg arising from a sequence of reactions, in either explosive C–N burning or convective He burning giving the net process ^{14}N$\rightarrow^{25}$Mg. In order for the ^{26}Al to be visible through its decay γ-ray, it must be carried or ejected from its place of production to optically thin regions in a time scale short compared to its halflife. In addition, destruction of ^{26}Al primarily by ^{26}Al(n, p)^{26}Mg or ^{26}Al(n,α)^{23}Na must be negligible; thus, the conditions for ^{26}Al formation are a proton-rich, neutron- poor environment. Detailed discussions of this problem have been given by Woosley (1986), Clayton and Leising (1987), Woosley (1991), Weaver and Woosley (1993). We summarize, briefly, the predicted yield of ^{26}Al to the ISM from several sources that have received serious consideration. We also include the recent proposal by Clayton (1994) that heavy cosmic ray interactions in molecular clouds are a possible contributor.

The Galactic distribution of several of the sources to be discussed is poorly known. Initially, Leising and Clayton(1985) have modeled the line emission using a distribution which is strongly peaked at the Galactic center to explain the *HEAO 3* and *SMM* observations. Higdon and Fowler (1989) have refined this model and calculated the angular distribution of the 1.809 MeV γ-ray for several modeled distributions which are broad, extending to more than a radian from the Galactic center. All modeled distributions were smooth except one which followed the distribution of molecular clouds which shows emission peaks at the Galactic center and at $\ell \sim 35°$.

It is clear that events on a Galactic scale such as novae, AGB objects, and massive stars (see below) which have a low intrinsic yield must occur frequently in the million year meanlife of ^{26}Al in order to produce a line intensity corresponding to the *COMPTEL* result for the Galactic center region. In this case the radiation distribution would be smooth.

It is important to remember, however, that any single nearby ($<$ 1 kpc) source of ^{26}Al should be considered as potentially capable of producing a measurable flux of the 1.809 MeV γ-ray line.

2.1. *AGB (Red Giants)*

Following the H and He core burning cycles, main sequence stars of initial mass $M < 10M_\odot$ evolve onto the AGB as red giants of radius (100–1000) $R_\odot$ with a hot white dwarf at its center (Iben 1989). Norgaard (1980) and Cameron (1984) suggested ^{26}Al production by what is called "hot bottom burning" (HBB) of H below the convective stellar envelope (Paulus and Forestini 1991). For stars with M$\sim$5–7 $M_\odot$ these estimates gave 2–3$\times10^{-5}$ $M_\odot$ of ^{26}Al per AGB star (Prantzos 1991) which is the maximum that could be injected into the ISM. Using the latest nuclear reaction cross-sections, recent calculations for AGB stars with $M = 3M_\odot$ and metallicity $Z = 0.03$, (Paulus and Forestini 1991; Forestini, Paulus, and Arnould 1991), show that $\sim 10^{-8}$ $M_\odot$ of ^{26}Al per AGB star could be added to the ISM after 13 thermal pulses. Extending these calculations to stars with main sequence masses 1–3 $M_\odot$, Forestini et al. (1991) estimate an average ^{26}Al yield of $\sim$0.1 $M_\odot$ injected into the ISM every million years. This result depends on several assumptions for the stars in this mass range which include a constant thermal interpulse separation and a constant dredge-up ^{26}Al mass per pulse, as well as on the initial mass function (IMF) adopted.

2.2. *Novae*

Numerous authors have suggested that thermonuclear nova outbursts are likely sites of ^{26}Al production. The current model of a nova outburst assumes that the event is generated by a thermonuclear runaway occurring on the surface of a white dwarf in hydrogen rich gas accreted from a companion, i.e., a cataclysmic binary system. Recent calculations by Starrfield et al. (1993) for accretion onto the surface of a (O-Ne-Mg) low mass ($\sim$1 $M_\odot$) white dwarf estimate a ^{26}Al yield of a few times 10^{-7} $M_\odot$ per nova, although Weiss and Truran (1990) predicted a yield more than an order of magnitude lower. It should be noted that it would require but a single local nova at a distance of 15 pc to produce the flux level observed by *COMPTEL* from the Vela region.

2.3. *Supernovae*

The supernovae source of ^{26}Al is expected to be from types SNe Ib and SNe II. These events are believed to result from the gravitational collapse of massive stars (M> 8$M_\odot$) at the end of the successive hydrostatic burning stages and may occur in either isolated or binary systems. The recent analysis of Thielemann et al. (1993) shows that O, Ne and Mg (the ^{26}Al seed nuclei) originate mostly in hydrostatic burning shells, with the amount ejected increasing rapidly with progenitor mass. Woosley (1991), considering in addition explosive neon burning and various neutrino processes (Woosley et al. 1990), shows that the ^{26}Al yield is generally increased over the presupernova value after the explosion for progenitor masses of 15-35 $M_\odot$ (see also Weaver and Woosley 1993). Prantzos (1993) has recently reviewed calculations of ^{26}Al production in massive stars including that from Wolf-Rayet stars of mass M>40$M_\odot$ (see §2.4 below). If Wolf-Rayet stars are the progenitors of Type Ib supernovae, then it is expected that still more ^{26}Al will be produced by explosive nucleosynthesis (see, for example, The et al. 1990). Among several other factors, the ^{26}Al yield depends on the presupernova metallicity which is a principal unknown in theoretical estimates of ^{26}Al production, since it depends on the Galactic locale, decreasing with Galactocentric radius (cf. Prantzos 1991, 1993). In Wolf-Rayet stars ^{26}Al may increase with metallicity (Prantzos and Casse 1986), but in SNe II it may actually decrease (Woosley and Weaver 1980). The extreme values for the ^{26}Al yield range from $2\times10^{-6}M_\odot$ to $4\times10^{-4}M_\odot$ for progenitor masses of $12M_\odot$ to $35M_\odot$, respectively.

2.4. *Wolf-Rayet Stars*

Another class of massive stars (M>30 $M_\odot$) are the Wolf–Rayet (WR) stars which show broad bright emission lines against a faint continuum. These stars are also characterized by low hydrogen and enhanced helium abundances and in some cases overabundance of N, C and O for the WN, WC and WO subclasses, respectively (Weiss and Truran 1992). These stars, near the main sequence, produce ^{26}Al through hydrostatic core H burning at temperatures above $T_c > 35\times10^6$ K (Dearborn and Blake 1985). In general, strong radiatively driven winds from the convective contracting core blow off a stellar envelope containing ^{26}Al. If the mass loss rate and extent of the convective core are sufficiently great then ^{26}Al can be injected into the ISM.

Recent calculations (Prantzos 1991), using the latest measured reaction rate for ^{25}Mg (p,γ) ^{26}Al, give ^{26}Al yields of 10^{-5} $M_\odot$ to $\sim$ 10^{-4} $M_\odot$ for stellar massses of 40 $M_\odot$ to 100 $M_\odot$. An average value of $\sim 4.5\times10^{-5}$ $M_\odot$ is found for M> 40 $M_\odot$ using a Salpeter IMF with index α=-2.5. These results are used along with an estimate of ^{26}Al from SNe II to estimate the total contribution from massive stars. An analysis by Prantzos (1993) concludes that WR stars can produce at most $\sim$20% of the Galactic ^{26}Al required, while SNe II and SNe Ib could produce half of it. (See also , Meynet and Arnould 1993.) Since these conclusions depend strongly on our knowledge of the WR

radial distribution (as well metallicity and the IMF), uncertainties remain substantial. Azzopardi (1992) points out that the number of identified Population I WR stars is only 161 compared to the estimated number of Galactic 1200 objects, based on surveys of these distinctive stars in other galaxies such as the LMC, SMC, and M31.

2.5. *A Nearby Supernova*

As seen from the above discussions, there are many possible sources for ^{26}Al, but uncertainties in the absolute yield predictions from nucleosynthesis calculations and the unknown spatial distributions of probable sources will make it difficult to interpret the ^{26}Al sky maps observed by *COMPTEL* in terms of sources distributed on a Galactic scale. In this regard it is important to recognize that local source(s) would reduce dramatically the required amount of radioactivity!

Some possibilities include: A nearby nova or supernova, nearby massive stars in the Wolf-Rayet phase, or, less likely, lower mass AGB stars. The first possibility is made likely by the X-ray evidence for a local interstellar bubble, presumably the result of a recent ($\lesssim 10^5$ years) nearby supernova (Cox and Anderson 1982; Cox and Reynolds 1987). The production requirements for ^{26}Al could be reduced by a factor of 10^4 for a local single source.

Dearborn and Blake (1985) have considered the possibility that the massive stellar winds from, e.g. Wolf-Rayet stars, could have enriched the local ISM with ^{26}Al. Morfill and Hartquist (1985) estimated the production of ^{26}Al in a "local" supernova superbubble which suggests again that $\sim 3-4$ M$_\odot$ of ^{26}Al may not be necessary to explain the observed flux of the 1.809 MeV line. More recently Blake and Dearborn (1989) have proposed a specific local source of ^{26}Al, Wolf-Rayets and supernovae production in OB stars in the Sco-Cen association. This model predicts a specific distribution of γ-rays in the sky and in particular a γ-ray signal at high Galactic latitude.

2.6. *Cosmic Ray/Molecular Cloud Interactions*

The γ-ray lines recently observed in the direction of the Orion molecular clouds (Bloemen et al. 1994) are presumed to arise from the interactions of heavy cosmic-rays ($Z > 2$) with the hydrogen and helium of the ISM. Such an explanation requires that the heavy cosmic-ray flux be enhanced by a factor of 30 over that in the solar neighborhood. Using this factor, Clayton (1994) has calculated the ^{26}Al abundance in the cloud from ^{26}Mg and ^{28}Si for (H,n) and (H, ppn) reactions, respectively. He also assumed that the abundances of Mg and Si relative to C - O in the Orion cloud correspond to those in the cosmic rays detected at the Earth and estimated that the production rate of ^{26}Al in the Orion complex could be 5.4×10^{51} atoms Myr^{-1}. For solar material and a cloud mass of 10^5 $M_\odot$, the ^{27}Al content is estimated as 2.6×10^{56} atoms, so the ^{26}Al/^{27}Al ratio in the cloud could be $\sim 2.1 \times 10^{-5}$. Previously Clayton had estimated that a smaller ^{26}Al/^{27}Al ratio of $\sim 10^{-6}$ was needed to obtain 2 $M_\odot$ of ^{26}Al in the entire ISM, approximately half of which is in molecular clouds (see Clayton 1994 and references therein). In principle then, cosmic ray spallation reactions in molecular clouds may also be considered as a contributor to the observed ^{26}Al.

3. Requirements for Future Experiments

The instruments that have been used to date for determining the distribution of the 1.809 MeV γ-rays do not directly provide a celestial image of the radiation. In a double-scatter type Compton telescope, such as *COMPTEL* , the incident direction of a γ-ray can only be determined to within a cone of half angle equal to the Compton scattering angle and with a resolution of several degrees for the conical shell thickness. The limitation on event topology and range of scattering angles

imposed by the two independent detectors of such a system results in a small effective area, and determining the proper background is a major problem. For example, one method of determining the background for the *COMPTEL* Galactic ^{26}Al line maps was based on the average of high latitude observations, which would be compromised by any local soure of celestial ^{26}Al (§2.5)), but other methods were also used. Complex Maximum Entropy or Maximum Likelihood methods convolved with the instrument response were finally necessary in order to extract the image from the background events. The line intensities in adjacent sky bins are then not truly independent as explained by Diehl et al. (1993a). In the case of the nonimaging, balloon-borne, *SMM* and *HEAO 3* spectrometers, a collimator defines the direction of a γ-ray signal above background to within an angle of typically 20°. Therefore, it is clear that a major advance in γ-ray imaging techniques is necessary to determine directly the celestial distribution of ^{26}Al.

In order to advance our knowledge of this important astrophysical problem we now describe a new imaging coded aperture γ-ray telescope which uses a liquid xenon detector for γ-ray spectroscopy and imaging. As will be demonstrated, the xenon detector can provide an ideal combination of high detection efficiency over a large area, good energy resolution, excellent spatial resolution, and event visualization capability which permits excellent background rejection. When used with a coded mask, the combination LXe-CAT gives a γ-ray telescope with excellent celestial angular resolution. The simultaneous image of the γ-ray sky and the background field with no assumptions about the source distribution can provide the information needed in order to determine the true nature of the source or sources of ^{26}Al.

3.1. *The Liquid Xenon-Coded Aperture Telescope (LXe-CAT)*

The proposed telescope (Aprile et al. 1992a) is shown schematically in Figure 1 along with a list of its principal characteristics. It combines a liquid xenon time projection chamber (LXe-TPC) as 3-D position sensitive γ-ray detector with a coded aperture mask to achieve precise measurement of the energy and angular distribution of γ-ray sources in the 0.3-10 MeV energy region. The coded mask is a 43×41 element uniformly redundant array (URA) of the type discussed in Fenimore and Cannon (1978). The size of the mask elements is 0.81 × 0.85 cm^2 with 1.2 cm thickness. With a detector-mask separation of 100 cm, the angular "pixel" is 0.46°×0.48° over a 19.3°×19.3° FOV. The telescope angular resolution is 30 arcminutes but point sources can be located with an accuracy as good as a few arcminutes, based on the excellent signal-to-noise ratio of the liquid xenon imaging detector. A larger mask-detector separation and/or smaller mask elements will give even more precise source location. The LXe detector is surrounded by an active anticoincidence shield to reduce the cosmic and atmospheric background γ-ray flux at balloon altitude. The active area of the LXe-TPC is 1200 cm^2. With an active liquid xenon layer of 10 cm (Z = 54, density = 3.06 g cm^{-3}), the full energy peak efficiency is about 65% at 1 MeV.

The LXe-TPC works on the principle that the free ionization electrons liberated in the liquid by a charged particle can drift under a uniform electric field, inducing a signal on sensing electrodes (see Figure 2). For a γ-ray, it is the electron resulting from a photoelectric absorption or a Compton scattering, or the electron-positron from a pair production, which will ionize and excite the xenon atoms yielding a large number of electron-ion pairs and scintillation photons (Doke et al. 1990, Kubota et al. 1977). The scintillation light signal is fast (< 10 ns), and thus an ideal marker of the time origin of a γ-ray interaction. From the measured electron drift time, referred to this time origin, and the known drift velocity, the coordinate of the interaction point, along the drift direction, is inferred. The other two coordinates, as well as the γ-ray energy, are inferred from the charge signals induced on the sensing electrodes. Thus the LXe-TPC measures both the energy and the spatial distribution of each ionizing event occurring within the sensitive volume. The factors which determine the ultimate energy and spatial resolution of a liquid xenon chamber have been

studied. Experimental results show that a submillimeter spatial resolution and a 6% FWHM energy resolution at 1 MeV can be realized in a practical detector (Aprile et al. 1991, 1992c). Improved energy resolution has been measured with liquid xenon doped with appropriate photosensitive materials (Ichinose et al. 1992; Aprile 1994a).

The intrinsic 3-D imaging capability of the LXe-TPC allows a direct visualization of the complex histories of γ-ray events with multiple interactions, initiated by either Compton or pair production, thus providing a powerful method for background identification and rejection. Using Compton kinematics, the original direction of a γ-ray undergoing multiple Compton scatterings in the liquid xenon can in fact be reconstructed from the measured energy and spatial coordinates of each scattering point. Events which kinematically could have not have come from the telescope's FOV are rejected as background. The signal-to-noise ratio can be further improved through the identification and rejection of background γ-rays interacting via photoabsorption or pair production, based on their location within the sensitive volume and their topology. The background rejection capability of the LXe-TPC, by Compton event reconstruction and by fiducial volume selection, has been demonstrated with Monte Carlo simulations (Aprile et al. 1993) and, more recently, with experimental results obtained with a 10 liter laboratory prototype (Aprile et al. 1994b).

The response of the LXe-TPC as a Compton polarimeter has also been studied, showing good sensitivity to polarization fractions as small as a few percent for strong sources, even in a balloon flight (Aprile et al. 1994a).

3.2. *The LXe-TPC as 3-D Position Sensitive Detector*

To image the ionization electrons produced by γ-ray interactions inside the sensitive volume of the LXe-TPC, we have proposed the system of sensing electrodes shown in Figure 2. The system consists of two orthogonal sense wire planes, separated from the drift region by a screening wire grid, and followed by a segmented plate anode. The presence of the grid means that a signal is induced on the sense wires only once the drifting electrons have crossed the grid.

The induction signal is positive while the electrons move toward the wires and negative while they drift away from the wires. The positions of the wires hit gives the $X - Y$ coordinates of the electron image. The drift time, referred to the zero time of the scintillation light trigger, plus the known drift velocity, provides the Z-coordinate information. The total event energy is measured from the charge collected on the plate anode. The idealized pulse shapes for a point-like charge moving in the drift region are also shown in Figure 2. While the induction signal on the wires is triangular in shape, the collection signal on the anode is step-like. For γ-ray events with multiple Compton interactions, the anode signal has a characteristic multi-step signature. The height of each step is proportional to the the energy liberated in the interaction point, and the time interval between the steps is proportional to the relative distance along the Z-direction between the interaction points. The sum of all the step pulse heights is proportional to the total energy of the original γ-ray, if it is totally absorbed.

The readout structure shown in Figure 2 is ideal for imaging the point-like charge clouds produced by MeV γ-rays in liquid xenon with a spatial resolution better than $d/\sqrt{12}$, where $d = 2$ mm is the sense wire spacing. This is due to the strong dependence of the induction signal amplitude on the lateral position of the charge cloud with respect to the sense wire (Gatti et al. 1970). The center of gravity of the image can then be determined from a weighted average of the signals induced on two adjacent wires, with an accuracy which depends on signal-to-noise. Other factors which influence the spatial resolution of the LXe-TPC are: 1) the physical extension of the charge cloud in the liquid, and 2) its diffusion during the drift. The intrinsic size of the charge cloud produced by 1 MeV ionizing radiation in liquid xenon, estimated by Monte Carlo, is on the order of 0.5 mm, which is not negligible compared with the detector's granularity. On the other hand, the spread

by diffusion of the center of gravity of a cloud of N electrons is given by $\sqrt{2Dt_d/N}$, where D is the diffusion coefficient and t_d is the drift time. Taking $D = 65\ \mathrm{cm^2 s^{-1}}$ (Shibamura et al. 1979), $t_d = 40\ \mu$sec as maximum drift time in the proposed LXe-TPC, and $N = 6.4 \times 10^4$ for 1 MeV ionizing radiation, the resulting diffusion spread is only 3 μm.

3.3. *Test Results with a 10 Liter LXe-TPC Prototype Detector*

To demonstrate the operation of a large liquid xenon detector, particularly spectroscopic and 3-D imaging capabilities, we have built and are currently testing a 10 liter LXe-TPC prototype, implemented with the electrode system discussed above (see Aprile et al. 1994b, Chen 1994). The prototype detector has half the drift gap, one third the sensitive area, and a volume similar to the sensitive volume of the proposed flight instrument. A spacing of 4 mm for the $X-Y$ wire planes was chosen to minimize the total number of electronics channels. Experiments have been carried out to test the cryogenics operation, the level of liquid xenon purity (which affects charge collection and thus energy resolution) and the imaging response to various γ-ray sources. We have verified that 10 liters of liquid xenon can be purified and maintained with a contamination level $\lesssim 1$ ppb over a period of several days. We have reproduced the energy resolution results previously obtained with smaller and simpler liquid xenon chambers. For the first time we have simultaneously measured the energy and the image of a collimated beam of γ-rays. Figure 3 shows the reconstructed image of 662 keV γ-rays from a ^{137} Cs source collimated with a 2 mm diameter hole. The data are consistent with a detector RMS spatial resolution better than 1 mm.

Event reconstruction based on Compton kinematics has also been demonstrated. A parallel vertical beam of γ-rays from a point source was simulated by placing a radioactive γ-ray source 40 cm above the detector's sensitive area. Events with a single Compton scattering followed by a photoabsorption were selected for this analysis. As an example, Figure 4 shows the on-line display of a 1.274 MeV γ-ray event from a ^{22}Na source-beam. The magnified view of the signal on the anode clearly shows a two-step event indicating that the γ-ray history was a Compton interaction followed by photoabsorption. The sum of the two steps pulse heights corresponds to the total energy of 1.274 MeV. From the time and amplitude analysis of the induction and collection signals, the coordinates and the energy for the two interaction points are inferred as well as their spatial separation. The most probable scattering angle is then found from the kinematics of the Compton scattering process. The accuracy on the angle determination depends on the spatial and energy resolution as well as on the separation between the two consecutive interaction points. Figure 5 shows the reconstructed event circles for nine ^{22}Na γ-ray events with a Compton scattering followed by photoabsorption. These experimental results directly demonstrate the LXe-TPC capability to identify and reject background via Compton event selection. In addition, they verify the feasibility of the original proposal (Aprile et al. 1989) to use a LXe-TPC as Compton/pair telescope for high energy γ-rays.

4. Monte Carlo Simulations

To demonstrate the capability of the LXe-CAT as an imaging γ-ray telescope, we have carried out Monte Carlo calculations that simulate the response of the instrument to several source distributions. In particular, we simulate the imaging process for a coded aperture imaging system in response to photon continuum spectra from point sources and to a γ-ray line from localized sources.

4.1. *Simulation of Coded Aperture Imaging*

Coded aperture imaging is related to the "multiple pinhole" technique (Dicke 1968). A planar absorber with a pattern of openings is placed between a γ-ray source and a position–sensitive detector. The absorber (or aperture) modulates the incident γ-ray flux, producing a response pattern on the position–sensitive detector. In general, the pattern is not a recognizable image of the source, so the pattern must be decoded or deconvolved to produce an image. Ideally, the imaging response to a point source should be a delta function with flat sidelobes. It has been shown (Fenimore and Cannon 1978) that a class of aperture patterns called Uniformly Redundant Arrays (URAs) has these properties. The source image can be reconstructed from the measured detector response pattern using a simple correlation calculation. The response pattern is correlated with a decoding function that is closely related to the aperture pattern. The correlation procedure is simply

$$S' = P * G \tag{1}$$

where S' is the reconstructed image, P is the detector response, G is the decoding function, and $*$ is the correlation operator. In terms of discrete arrays,

$$S'(i,j) = \sum_{k=1}^{r} \sum_{l=1}^{s} P(k,l) G(i+k, j+l) \tag{2}$$

where r and s are the dimensions of the (rectangular) aperture pattern. A review of the properties of coded aperture imaging can be found in Caroli et al. (1987).

The LXe detector is simulated as an active volume of liquid xenon (density = 3.06 g cm^{-3}) that is 35 cm×35 cm and 10 cm thick. The calculations also simulate inactive xenon around the sensitive volume in the detector container, and a 5 cm thick CsI shield surrounding the LXe detector and extending 20 cm above the top face. The coded aperture mask is modeled as a URA pattern of blocks of tungsten alloy (90% W and 10% Cu, density = 17.0 g cm^{-3}). The exact pattern that is used depends on the desired angular resolution.

For our simulations, we choose a mask design and a mask/detector separation that will give sub-degree angular resolution over a reasonably wide field-of-view (FOV). In this case, the basic mask pattern is a 43 × 41 element URA at a distance of 100 cm from the LXe detector face.

Monte Carlo histories are generated for γ-rays incident on the telescope at energies between 0.3 and 10 MeV. Photoelectric, Compton, and pair events are identified and recorded. Secondary electrons, resulting from γ-ray interactions, are assumed to lose all their energy at the point of creation if their kinetic energy is less than 2 MeV. The program also includes the uncertainties in the interaction location and in the energy loss at the interaction point due to the detector's finite spatial and energy resolution.

A point source of γ-rays is simulated by a parallel beam of photons that is uniformly distributed over the active area of the detector. The program checks for interactions in the mask and the active xenon volume, as well as in other sections of the instrument. The program records the location of interactions and follows the histories of the secondary γ-rays and electrons. An inventory is also kept of the energy depositions within the active xenon volume. For events with multiple interaction points, the algorithm based on Compton kinematics is used to determine which was most likely to be the point of the first interaction (e.g., Aprile et al. 1993), since this information is required for the imaging process.

We simulate the background in the shielded LXe detector with a random distribution of counts throughout the detector volume. The number of background counts is determined by the detector efficiency, the background flux expected in the operating environment, and the observation time.

The following components of the continuum instrumental background were considered to estimate the total background count rate in the LXe-CAT at balloon altitude: 1) aperture flux; 2) shield leakage; 3) elastic neutron scattering; 4) spallation products; and 5) background from the coded aperture mask. Cosmic diffuse and atmospheric γ-rays are the major sources that contribute to components 1) and 2) at balloon altitudes. The parameterized form of the atmospheric γ-ray spectrum given by Costa et al. (1984) and the cosmic diffuse spectrum given by Schönfelder, Graser and Daugherty (1977) were used. The neutron spectrum inside the LXe detector was taken from Gehrels (1985). For the spallation spectrum, we used the spectrum from Dean, Lei, and Knight (1991) scaled to the LXe density and mass number. The background from the tungsten mask (due mainly to secondary photons from the interaction of atmospheric γ-rays in the mask) has been estimated using the empirical formula of Owens et al. (1985, see also Dunphy et al. 1989). Background in the LXe-CAT instrument in a low Earth orbit was also estimated using the techniques described in Gehrels (1992).

Figure 6 shows the calculated total background spectrum and its individual components at 3 g cm^{-2} over Palestine, Texas. To reduce the background, we apply the event reconstruction algorithm based on Compton kinematics discussed in Aprile et al. (1993). At 2 MeV the estimated count rate is reduced by a factor of ~ 2 when events which kinematically could not have entered the aperture defined by the shield ($\sim 50°$) are rejected. By applying a more stringent software collimation of only 3°, for the case of a very narrow FOV, the background is reduced by almost an order of magnitude. For a detailed description of the background calculations and the effective reduction of background events in the MeV region we refer to Aprile et al. 1994c.

In general, the background in the detector will not be distributed uniformly throughout the sensitive volume. If not accounted for, this will cause a false structure to appear in the reconstructed image. In practice, this false structure can be removed by making a background observation under similar conditions for a time equal to the source observation time. The background pattern in the position sensitive volume can then be used to correct the source observation, cancelling out the structure due to the background non-uniformity. Because of the background subtraction, however, the effective background (i.e., its variance) is increased by a factor of 2. This approach has been used successfully in balloon flights of a coded aperture γ-ray detector (Dunphy et al. 1989; Bhattacharya 1990).

The source plus background simulation produces a distribution of event locations in the detector. The locations are binned to match the dimensions of the mask elements (i.e., an $r \times s$ array), producing the array $P(k,l)$ in equation (2). The correlation of this array with the decoding array, G, produces an image of the source, S'.

4.2. *Simulation Results*

4.2.1. *The Crab Nebula Region*

To illustrate the response of the LXe-CAT to continuum spectra of γ-rays from discrete sources, we simulate the Crab Nebula. The differential photon spectrum is a power law of the form (Penningsfeld, Graser and Schönfelder 1979)

$$dN/dE = 3 \times 10^{-3} E_{MeV}^{-2.3} \mathrm{cm}^{-2}\mathrm{s}^{-1}\mathrm{MeV}^{-1}. \quad (3)$$

First, we simulate images from a typical high-altitude balloon observation. The source observation time is taken to be 10 hours, with an equal length of time taken for measurement of background non-uniformity. The background shown in Figure 6, reduced by a factor of ~ 2 after Compton event reconstruction, is applied. This corresponds to the background rejection expected for a 19°

FOV. Absorption of source photons by the residual atmosphere at a depth of 3.0 g cm^{-2} is included in the calculations. The effective increase in background (a factor of 2) required by the evaluation of background non-uniformity is also taken into account. Images resulting from the simulation in two energy ranges are shown in Figure 7. The source is present at a significance level of 16σ in the range 0.5–1 MeV (Figure 7a) and 11σ in the range 1–10 MeV (Figure 7b). Since a point source can be located with a precision of (McConnell et al. 1987)

$$\sigma_{loc} = \sigma_{pixel}/n_{\sigma} \tag{4}$$

and the characteristic size of a pixel is about 30′, the uncertainty in the Crab Nebula location for this observation would be about 2′.

To illustrate the capability of the same detector to resolve separate point sources in the same FOV, we simulate a satellite-based observation of the Crab Nebula and the quasar PKS0528+134. For the γ-ray spectrum from the quasar, we use the most intense spectrum > 3 MeV consistent with the *COMPTEL* observations reported by Collmar et al. (1993). The live-time is taken to be 2 weeks and the background for a low Earth orbit is used. The image in the energy range 3–20 MeV is shown in Figure 8. PKS 0528+134 is seen in the image at a significance level of 6σ.

4.2.2. *The Galactic Center and Vela Regions*

As discussed in §1, the measurement of the ^{26}Al distribution in the Galaxy via the 1.809 MeV γ-ray line is an extremely important objective for γ-ray astronomy. For the 1.809 MeV source distribution, we use the maps of this radiation observed by *COMPTEL* (Diehl et al. 1994c). These maps show a highly structured emission over a wide longitude range with "hot spots" scattered along the Galactic plane, especially near the Galactic center and in the direction of the Vela and Cygnus regions.

For the Galactic center "hot spot" we use the flux of 3.6 $\times 10^{-4}$ cm^{-2} s^{-1} reported by Diehl et al. (1994b) and assume a "point source" distribution (i.e., less than about 0.5° in extent, the intrinsic angular resolution of the simulated detector). We assume a satellite-based observation time of 1344 hr. This corresponds to the *COMPTEL* observation live-time ($\sim$ 8 weeks). The simulated image for these conditions is shown in Figure 9. The significance of the galactic center "hot spot" is about 13σ. This compares favorably with the 6.5σ significance of this source for *COMPTEL* (Diehl et al. 1993). The Vela "hot spot," with a flux of 2.2 $\times 10^{-5}$ cm^{-2} s^{-1}, would have a significance of 9σ in the LXe-CAT for the same observing conditions.

We note that if the source is extended in size such that the flux is divided equally among n image pixels, the source significance in *each* pixel will be reduced by a a factor of n. An improved response to extended emission can be achieved by a modified LXe-CAT configuration or by removing the coded aperture and using the LXe-TPC as a Compton telescope.

5. Conclusions

We have described the design of a unique γ-ray imaging telescope operating in the energy range 0.3–10 MeV. The telescope is based on a liquid xenon time projection chamber (LXe-TPC). Location and energy analysis of events with multiple Compton scatterings in the liquid permits to use Compton kinematics to reconstruct the possible directions of the incident photon. This will allow significant reduction of background. Use of fiducial volume cuts will also allow background reduction for single scattering events and internal β-decays.

Another major benefit of using a TPC is that the heavy external shielding usually added to attenuate background can be eliminated or greatly reduced because of the background reduction

techniques allowed by the intrinsic 3-D imaging. By combining the LXe-TPC with a coded mask we obtain an imaging telescope (LXe-CAT) with superior celestial angular resolution and source localization accuracy over other instruments. We have chosen to demonstrate the capabilities of this new instrument by performing simulations for a satellite observation of localized sources of 1.809 MeV ^{26}Al identified by *COMPTEL*. Since it is essential to verify the properties of a new telescope design with a balloon test flight, we have also performed a simulation of a balloon-based observation of the Crab Nebula γ-ray spectrum.

Considerable work has been done at the Columbia University Astrophysics Laboratory to assess the feasibility of a liquid xenon chamber for γ-ray imaging and spectroscopy. A 10 liter LXe-TPC prototype has been developed and tested in the laboratory. A first balloon flight of a LXe-CAT to observe the Crab Nebula and verify the instrument's imaging capability and the background in a space environment could be carried out within two years.

ACKNOWLEDGEMENTS

This work was supported by a NASA grant (NAGW-2013) to the Columbia Astrophysics Laboratory.

REFERENCES

Aprile, E., Mukherjee, R., & Suzuki, M. 1989, SPIE Proc., 1159, 295
Aprile, E., Mukherjee, R., & Suzuki, M. 1991, Nucl. Instr. and Meth., A302, 177
Aprile, E., Bolotnikov, A., Chupp, E., & Dunphy, P. 1992a, NASA proposal, CAL-2015
Aprile, E., Chen, D., Moulson, M., Mukherjee, R., & Suzuki, M. 1992c, Nucl. Instr. and Meth., A316, 29
Aprile, E., Bolotnikov, A., Chen, D., & Mukherjee, R. 1993, Nucl. Instr. and Meth. A327, 216
Aprile, E., Bolotnikov, A., Chen, D., Mukherjee, R., & Xu, F. 1994a, ApJS, 92, 689
Aprile, E., Bolotnikov, A., Chen, D., Muhkerjee, R., & Xu, F. 1994b, SPIE Proc. 2305, 33
Aprile, E., Bolotnikov, A., Chen, D., & Xu, F., 1994c, Nucl. Instr. and Meth. (in preparation)
Arnett, W. D. 1977, Ann. N.Y. Acad. Sci. 302, 90
Azzopardi, M. A. 1992, in The Astronomy and Astrophysics Encyclopedia, ed. S.P. Maran, (New York: Van Nostrand Reinhold), 812
Bhattacharya, D. 1990, Unpublished Ph.D. thesis, University of New Hampshire
Blake, J.B., Dearborn, P.S. 1989, ApJ, 338, L17
Bloemen, H. et al. 1994, A&A, 281, L5
Cameron, A.G.W. 1984, Icarus, 60, 416
Caroli, E., Stephen, J.B., Di Cocco, G., Natalucci, L., & Spizzichino, A. 1987, Space Sci. Rev. 45, 349
Chen, D. 1994, Unpublished Ph.D. thesis, Columbia University
Clayton, D.D. 1984, ApJ, 280, 144
Clayton, D.D. 1994, Nature, 368, 222
Clayton, D.D., & Leising, M.D. 1987, Physics Reports, 144, 1–50
Collmar, W., Bloemen, H., Bennett, K., Diehl, R., Hermsen, W., McConnell, M., Lichti, G.G., Ryan, J., Schönfelder, V., Stacy, J.G., Steinle, H., Strong, A., & Williams, O.R. 1993, Proc. 23rd ICRC 1, 168
Costa, E., Massaro, E., Salvati, M., & Appolloni, A., Astrophys. Space Sci. 100, 165
Cox, D.P., & Anderson, P. R., 1982, ApJ, 253, 268
Cox, D.P., & Reynolds, R. J., 1987, ARA&A, 25, 303

Dean, A.J., Lei, F., & Knight, P.J. 1991, Sp. Sci. Rev., 57, 109
Dearborn, D.S.P., & Blake, J.B. 1985, ApJ, 288, L21
Diehl, R., et al. 1993a, A&AS, 97, 181
Diehl, R., et al. 1993b, Adv. Space Res., 13, 723
Diehl, R., et al. 1993c, AIP Conf. Proc., 280 ed. N. Gehrels, (AIP:New York), 40
Diehl, R., et al. 1993d, 23rd Int. Cos. Ray Conf. (Calgary) 1, 136
Diehl, R., et al. 1994a, ApJS, 92, 429
Diehl, R., et al. 1994b, AIP Conf. Proc., 304, ed. C. Fichtel, (AIP: NY) 147
Diehl, R., et al. 1994c, A& A, in press
Dicke, R.H. 1968, ApJ, 153, L101
Doke, T., Musuda, K., & Shibamura, E. 1990, Nucl. Instr. and Meth., 291, 617
Dunphy, P.P., McConnell, M.L., Owens, A., Chupp, E.L., Forrest, D.J., & Googins, J. 1989, Nucl. Instr. and Meth. A274, 362
Fenimore, E.E., & Cannon, T.M., 1978, Appl. Opt., 17, 337
Forestini, M., Paulus, G., & Arnould, M. 1991, A&A, 252, 597
Gatti, E., et al. 1970, IEEE Trans. Nucl. Sci. NS-26, 2910
Gehrels, N. 1985, Nucl. Instr. and Meth., A239, 324
Gehrels, N. 1992, Nucl. Instr. and Meth., A313, 513
Higdon, J.C., & Fowler, W.A. 1989, ApJ, 339, 956
Iben, I., Jr. 1989, "Peculiar Red Giants – What Kind of White Dwarfs Do they Become?" in Evolution of Peculiar Red Giant Stars, eds. H. R. Johnson and B. Zuckerman, (Cambridge: Cambridge University Press), 205
Ichinose, H., Doke, T., Hitachi, A., Kikuchi, J., Masuda, K., & Shibamura, E. 1992, Nucl. Instr. & Meth., A322, 216
Kubota, S., Suzuki, & M., Ruan(Gen), J. 1979, Phys. Rev. B, 20, 3486
Leising, M.D., & Clayton, D.D. 1985, ApJ, 294, 591
Malet, I, et al. 1991, in Gamma-Ray Line Astrophysics (AIP Conf. Proc. 232) eds., P. Durouchoux and N. Prantzos (New York, AIP), 123
MacCallum, C.J., Huters, A.F., Stang, P.D., & Leventhal, M. 1987, ApJ, 317, L12
Mahoney, W. A., Ling, J.C., Wheaton, W.A., & Jacobsen, A.S., 1984 ApJ, 286, 578
McConnell, M.L., Dunphy, P.P., Forrest, D.J., Chupp, E.L., & Owens, A. 1987, ApJ, 321, 543
Meynet, G., & Arnould, M., 1993 in Origin and Evolution of the Elements, eds. N. Prantzos, E. Vangioni-Flam & M. Cassé, (Cambridge:Cambridge University Press), 539
Morfill, G.E., & Hartquist, T.W., 1985, ApJ, 297, 194
Norgaard, H. 1980, ApJ, 236, 895
Oberlack, U., Diehl, R., Montmerle, T., Prantzos, N., & von Ballmoos, P. 1994, ApJS, 92, 433
Owens, A., Frye, Jr., G.M., Hall, C.J., Jenkins, T.L., Pendleton, G.N., Carter, J.N., Ramsden, D., Argrinier, B., Bonfand, E., Gouiffes, C., & Tabary, A. 1985, Proc. 19th ICRC 3, 314
Paulus G., & Forestini, M., 1991, in Gamma-Ray Line Astrophysics (AIP Conference Proceedings # 232), eds. P. Durouchoux & N. Prantzos (New York: AIP), 183
Penningsfeld, F.–P., Graser, U., & Schönfelder, V. 1979, Proc. 16th ICRC 1, 101
Prantzos, N., 1991, in Gamma-Ray Line Astrophysics (AIP Conference Proceedings # 232), eds. P. Durouchoux & N. Prantzos (New York: AIP), 129
Prantzos, N., 1993, ApJ, 405, L55
Prantzos, N., & Cassé, M. 1986, ApJ, 307, 324
Ramaty, R., & Lingenfelter, R.E. 1977, ApJL, 213, L5
Schönfelder, V., Graser, U., & Daugherty, J., ApJ, 217, 306 (1977)
Share, G.H., Kinzer, R.L., Kurfess, J.D., Forrest, D.J., Chupp, E.L., & Rieger, E. 1985, ApJ, 292, L61

Starrfield, S., Shore, S.N. Sonneborn, G., Gonzalez - Riestra, R., Sparks, W.M., Truran, J.W., Dopita, M.A., & Williams, R.E., 1993, AIP Conf. Proc. 280, 168

Teegarden, B.J., Barthelmy, S.D., Gehrels, N., Tueller, J., Leventhal, M., & MacCallum, C.J. 1991, ApJ, 375, L9

The, L.-S., Clayton, D.D., & Burrows, A. 1990, Arizona Theoretical Astrophysical Preprint # 90-20

Thieleman, F.-K., Nomoto, K., & Hashimoto, M., 1993 in Les Houches Lectures, Supernovae," ed. R. Mochkovitch, in press

Varendorff, M., & Schönfelder, V. 1992, ApJ, 395, 158

Von Ballmoos, P., Diehl, R., & Schönfelder, V. 1987, ApJ, 318, 654

Weaver, T.A., & Woosley, S.E., 1993, Phys. Rep. 227, 65

Weiss, A. & Truran, J.W., 1990, A&A, 238, 178

Weiss, A. and Truran, J.W., 1992, "Stellar Evolution, Massive Stars" in The Astronomy and Astrophysics Encyclopedia, ed. S.P. Maran (Van Nostrand Reinhold: New York), 839

Woosley, S.E., 1986, in Nucleosynthesis and Chemical Evolution, eds. B. Hauck, A. Maeder & G. Meynet (Springer Verlag: Berlin), 78

Woosley, S.E., & Weaver, T.A., 1980, ApJ, 238, 1017

Woosley, S.E., Hartmann, D.H., Hoffman, R.D., & Haxton, W. C., 1990, ApJ, 356, 272

Woosley, S. E., 1991, in Gamma-Ray Line Astrophysics, eds. P. Durouchaux & N. Prantzos, AIP Conf. Proc., 232, (AIP: NY), 270

FIGURE CAPTIONS

Figure 1. Schematic view of the Liquid Xenon-Coded Aperture Telescope (LXe-CAT).

Figure 2. Schematic view of the electrodes system for the three dimensional Liquid Xenon-Time Projection Chamber (LXe-TPC).

Figure 3. Two-dimensional spatial distribution of 662 keV γ-rays from a collimated ^{137}Cs source as detected by the 10 liter LXe-TPC prototype. The collimator diameter is 2 mm.

Figure 4. The on-line display of a Compton scattering event recorded in the 10 liter LXe-TPC prototype, showing the digitized induction signals and anode signal. The anode signal has been magnified to show the double interaction signature of the event.

Figure 5. Reconstructed event circles are shown for nine Compton scattering events from a point source of ^{22}Na 1.274 MeV γ-rays. The celestial sphere is subdivided into $5° \times 5°$ bins and the source location is at $0° \times 0°$.

Figure 6. The estimated differential background count rate spectrum and its components are shown for the LXe-CAT at balloon altitude (3 g cm^{-2}) over Palestine, Texas. The LXe-CAT was shielded with 5 cm of CsI and no "software" background rejection was applied.

Figure 7. A simulated image of the Crab Nebula is shown for a 10 hr balloon observation. a) image in 0.5–1 MeV energy range (16σ significance); b) image in 1–10 MeV range (11σ significance).

Figure 8. A simulated image of the Crab Nebula and quasar PKS 0528+134 in the 3–20 MeV energy range is shown for a 336 hr satellite observation. PKS 0528+134 is significant at a level of 6σ.

Figure 9. A simulated image of the ^{26}Al "hot spot" near the Galactic center at the energy 1.809 MeV is shown for a 1334 hr satellite observation. The source is significant at a level of 13σ.

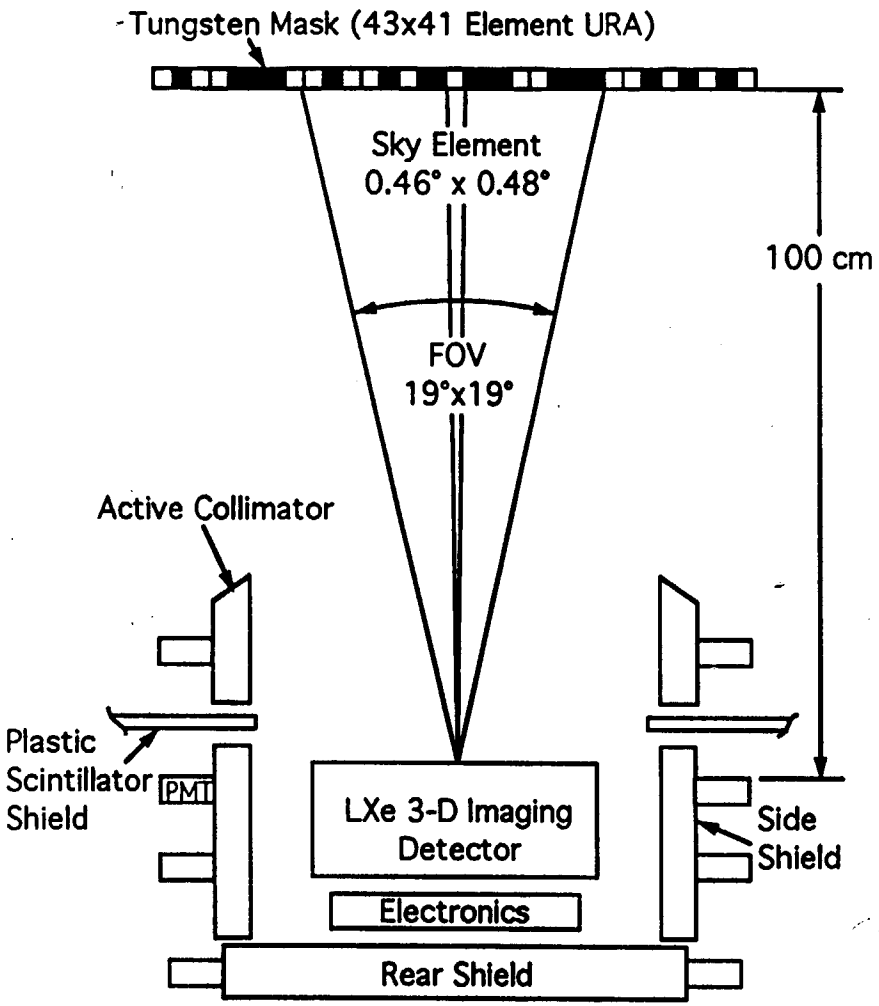

LXe-CAT Properties

Energy Range	0.3 - 10 MeV
Energy Resolution	5.9% FWHM at 1 MeV
3-D Spatial Resolution	< 1 mm RMS
Geometrical Area	~1200 cm^2
Active Shield	5 cm CsI
FOV (Fully Coded)	19° x 19° FWHM
Angular Resolution	30 arcmin
Point Source	
Location Accuracy	~2 arcmin(10σ source)
Min Flux (Line)	8 x10^{-5} ph cm^{-2} s^{-1}
3σ at 1 MeV	(3 x 10^4 s)
Min Flux (Continuum)	3 x 10^{-7} ph cm^{-2} s^{-1} keV^{-1}
3σ at 1 MeV	(3 x 10^4 s)

Fig. 1

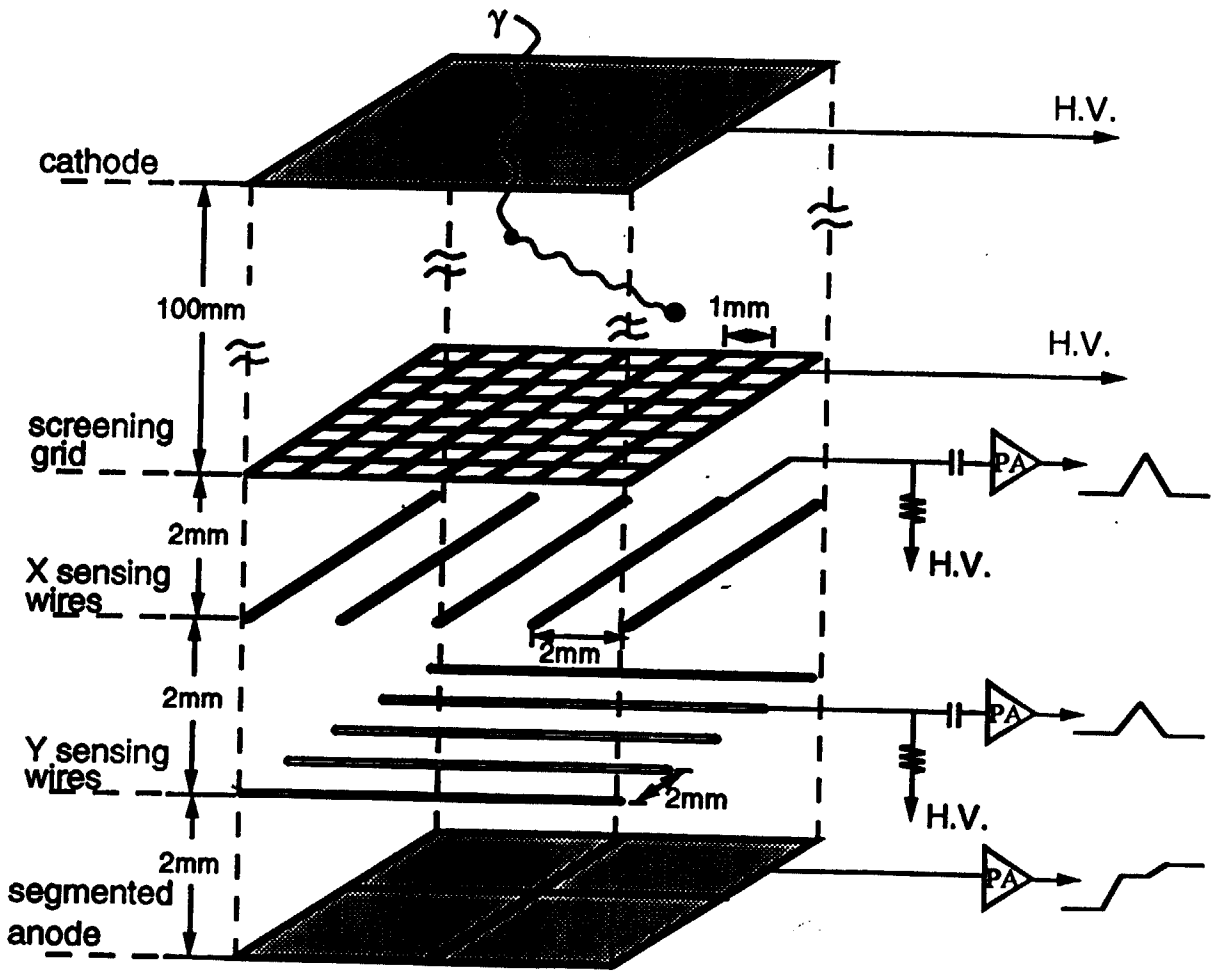
γ
cathode
H.V.
100mm
1mm
H.V.
screening grid
PA
2mm
X sensing wires
H.V.
2mm
2mm
Y sensing wires
PA
2mm
H.V.
2mm
segmented anode
PA

Fig. 2

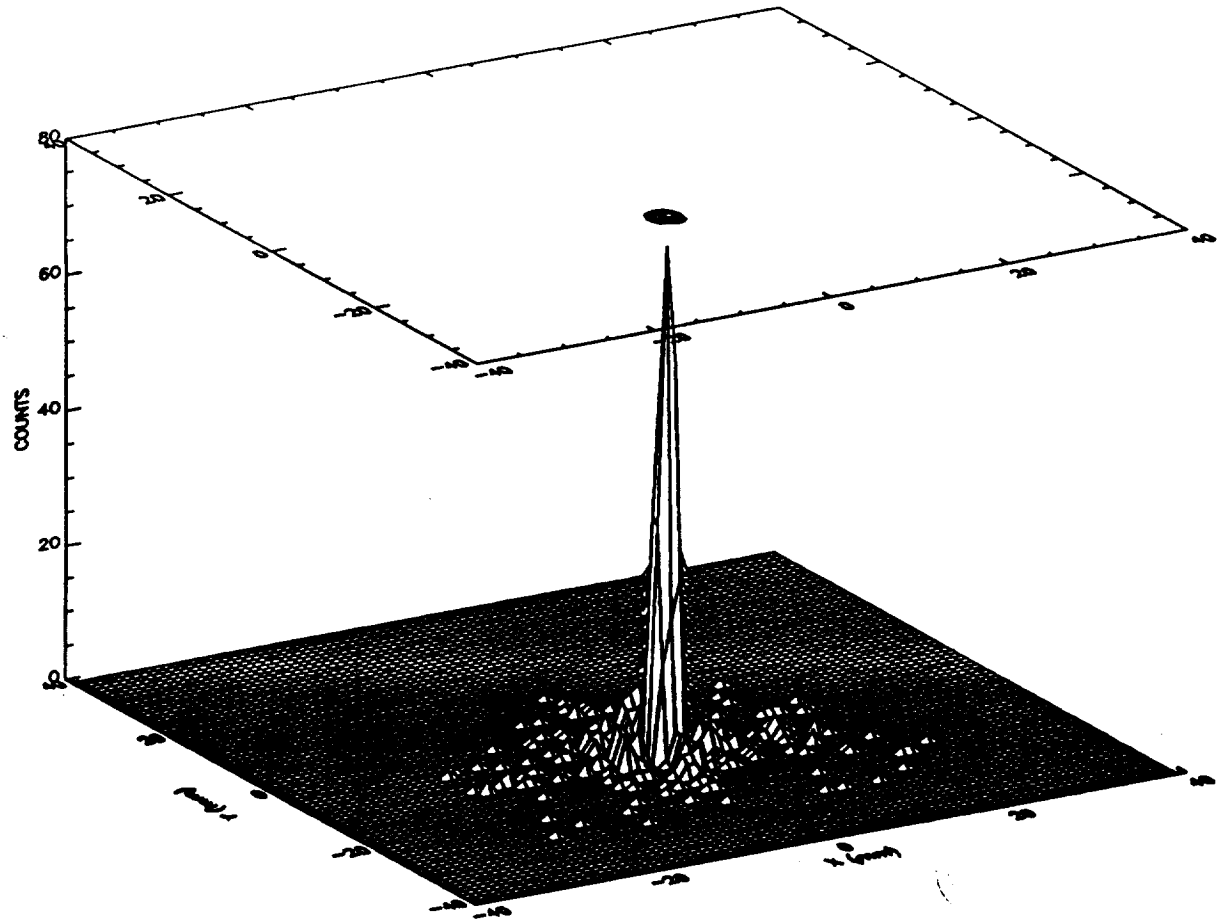

Fig. 3

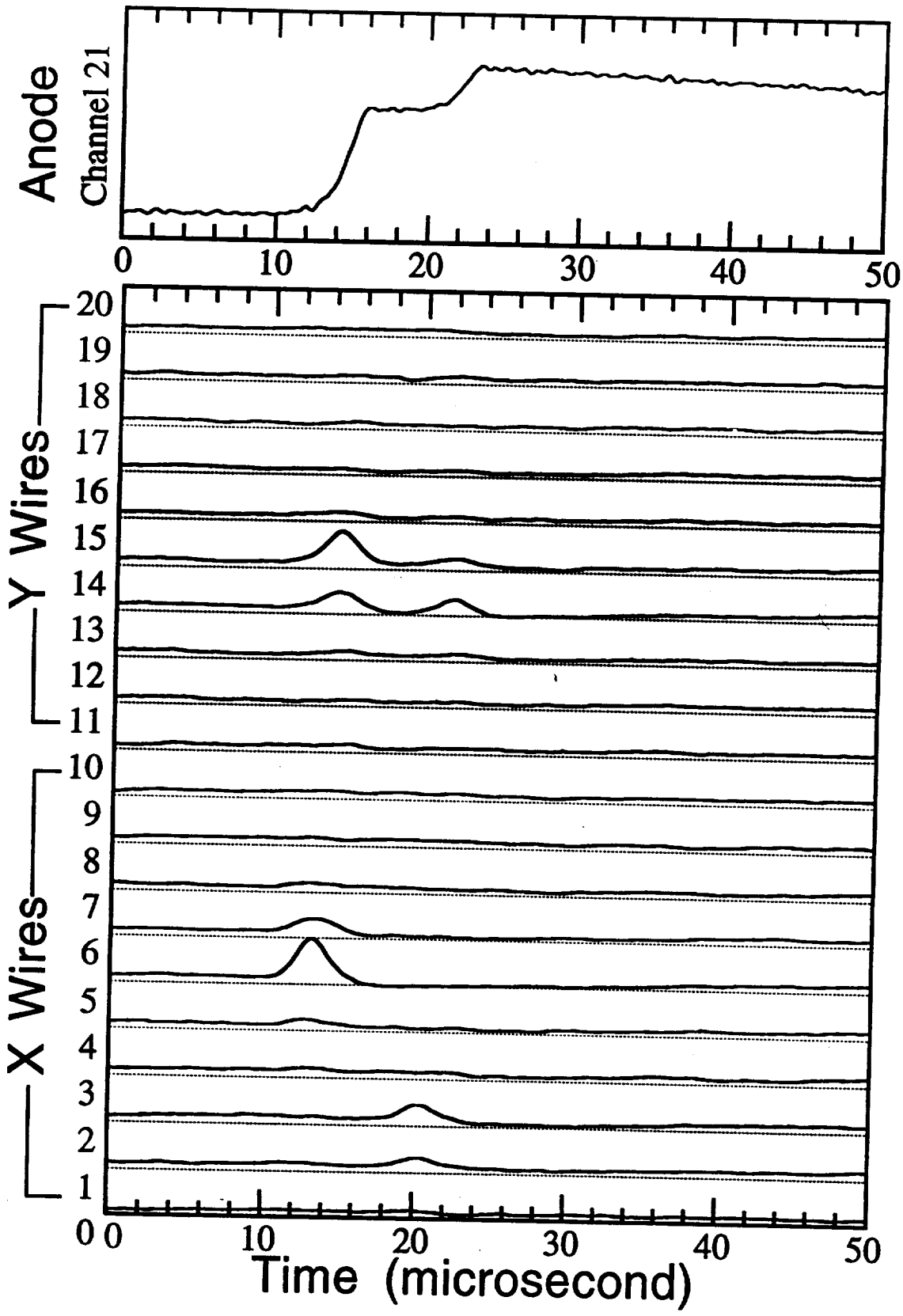
Anode
Channel 21
0
10
20
30
40
50
Y Wires
20
19
18
17
16
15
14
13
12
11
X Wires
10
9
8
7
6
5
4
3
2
1
0
0
10
20
30
40
50
Time (microsecond)

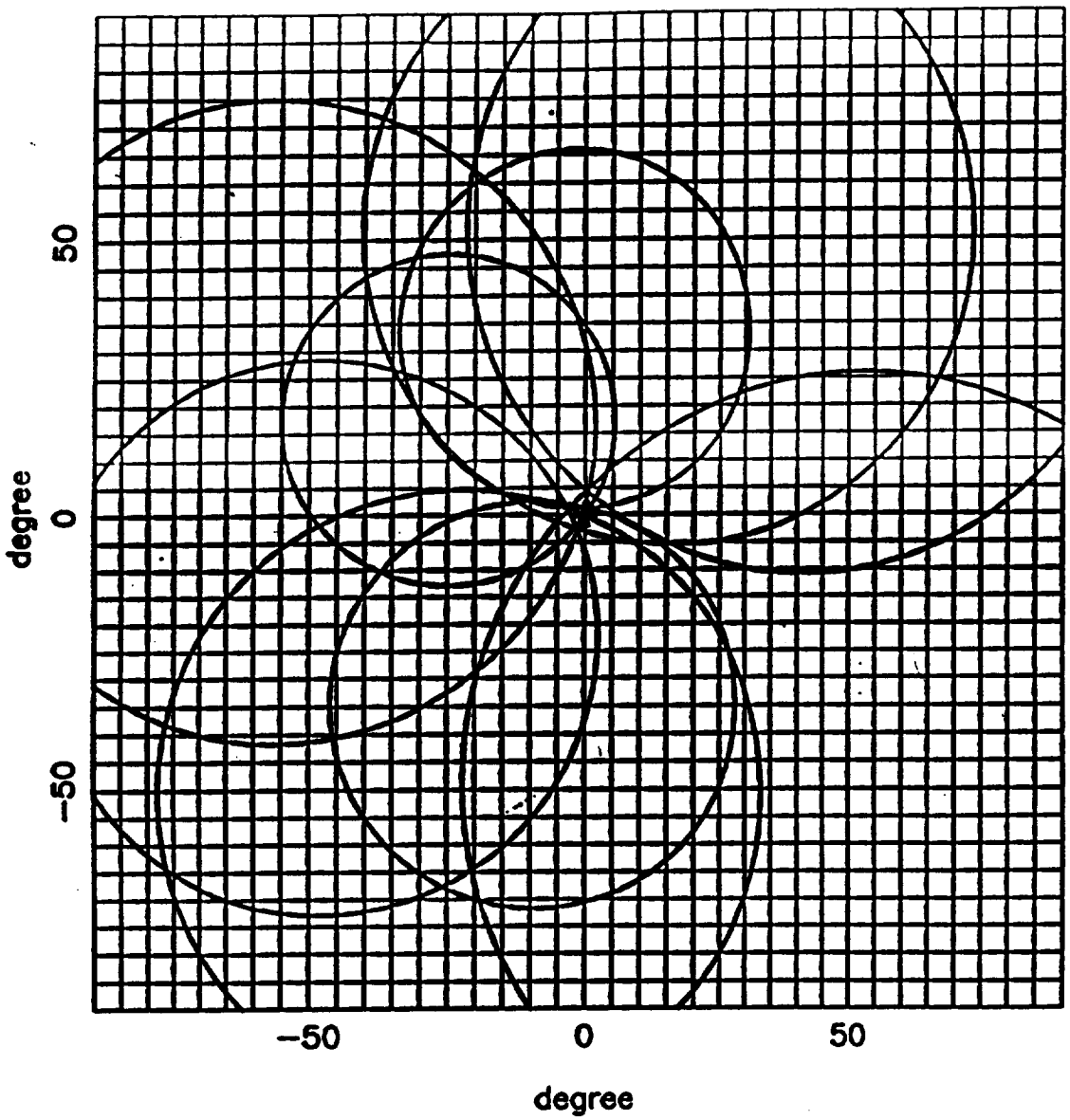

Fig. 5

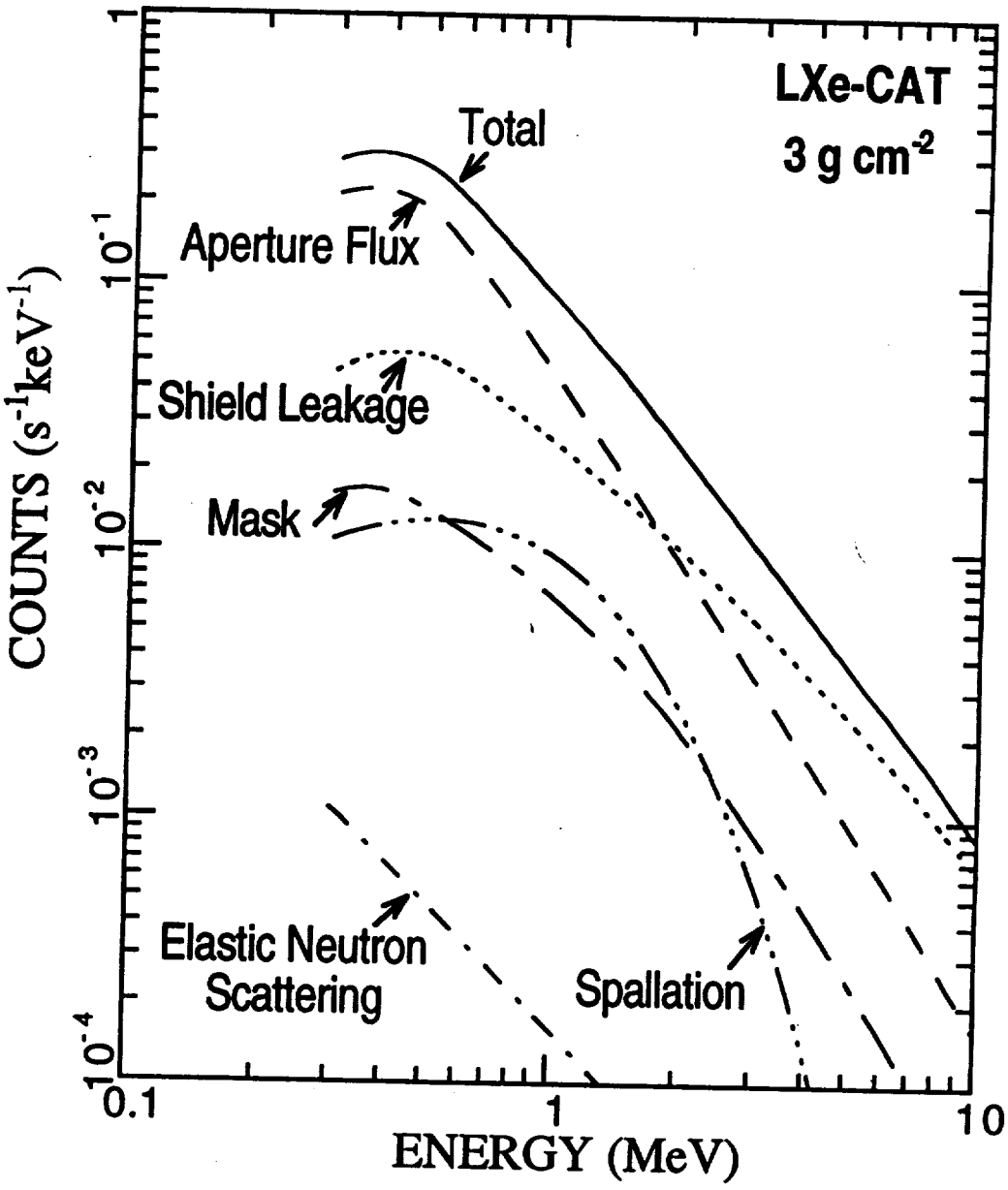
LXe-CAT
3 g cm-2
Total
Aperture Flux
Shield Leakage
Mask
Elastic Neutron Scattering
Spallation
COUNTS (s-1keV-1)
ENERGY (MeV)
1
10-1
10-2
10-3
10-4
0.1
1
10

Fig. 6

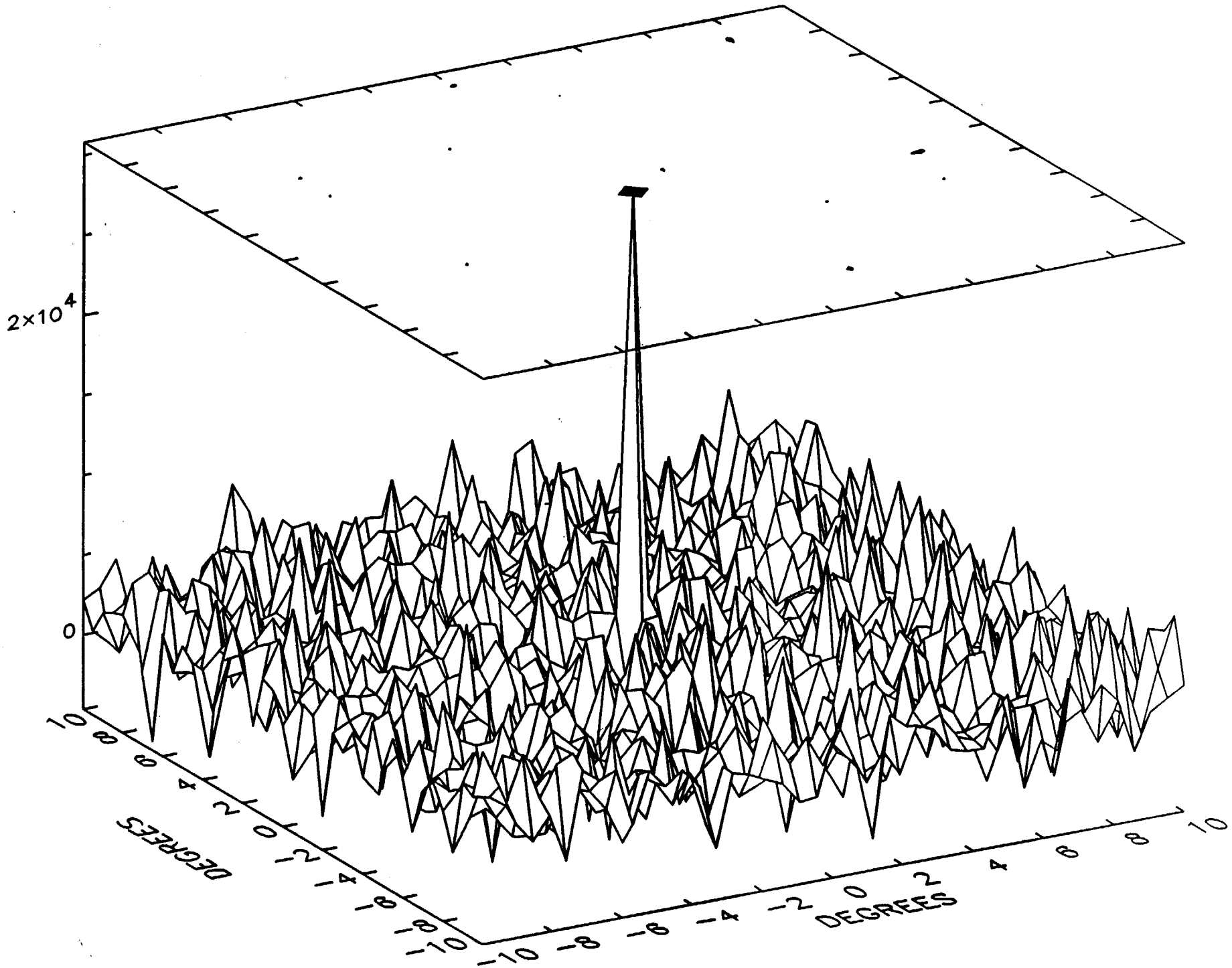

Fig. 7a

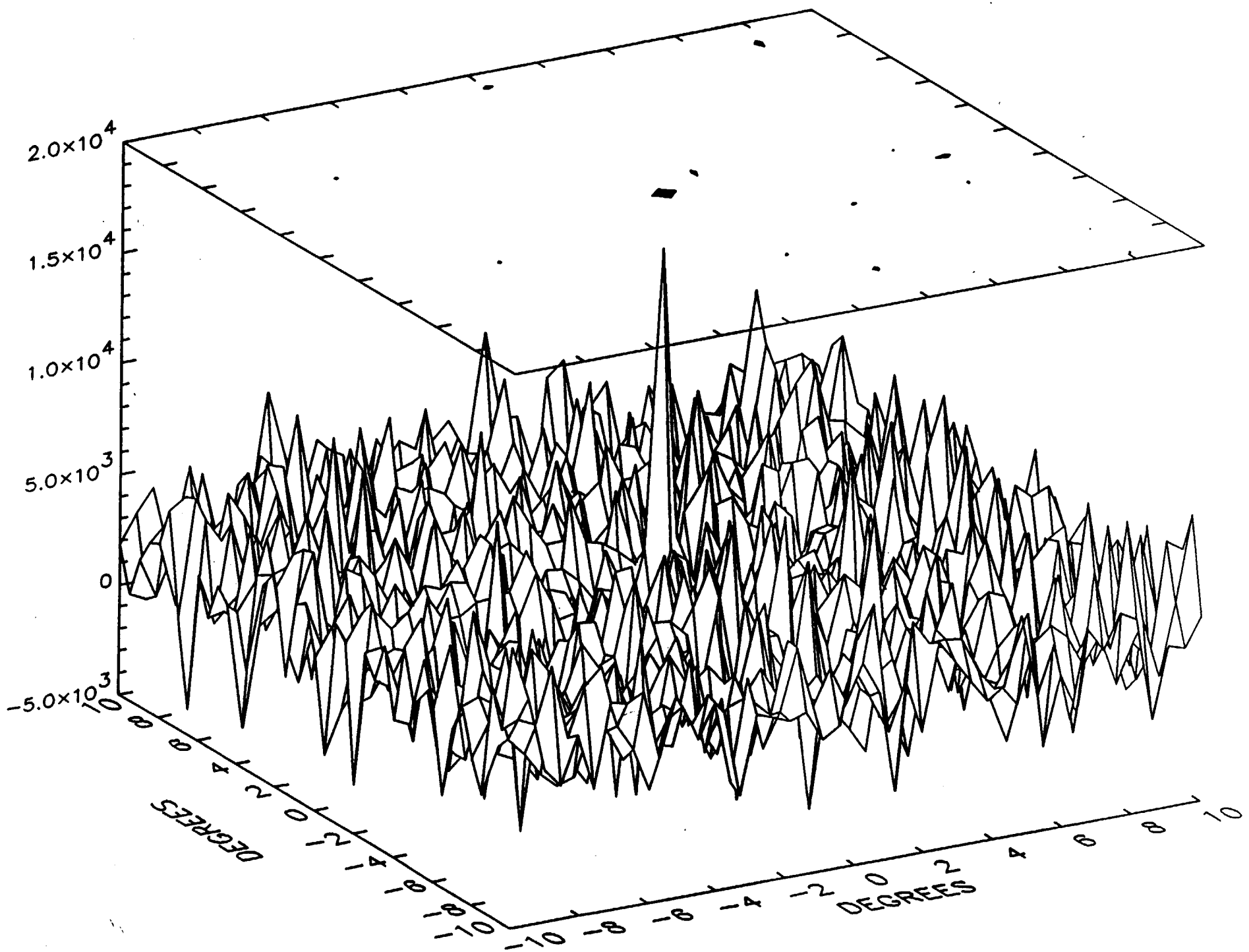
2.0×10^4
1.5×10^4
1.0×10^4
5.0×10^3
0
-5.0×10^3
10
8
6
4
2
0
-2
-4
-6
-8
-10
DEGREES
-10 -8 -6 -4 -2 0 2 4 6 8 10
DEGREES

Fig. 7b

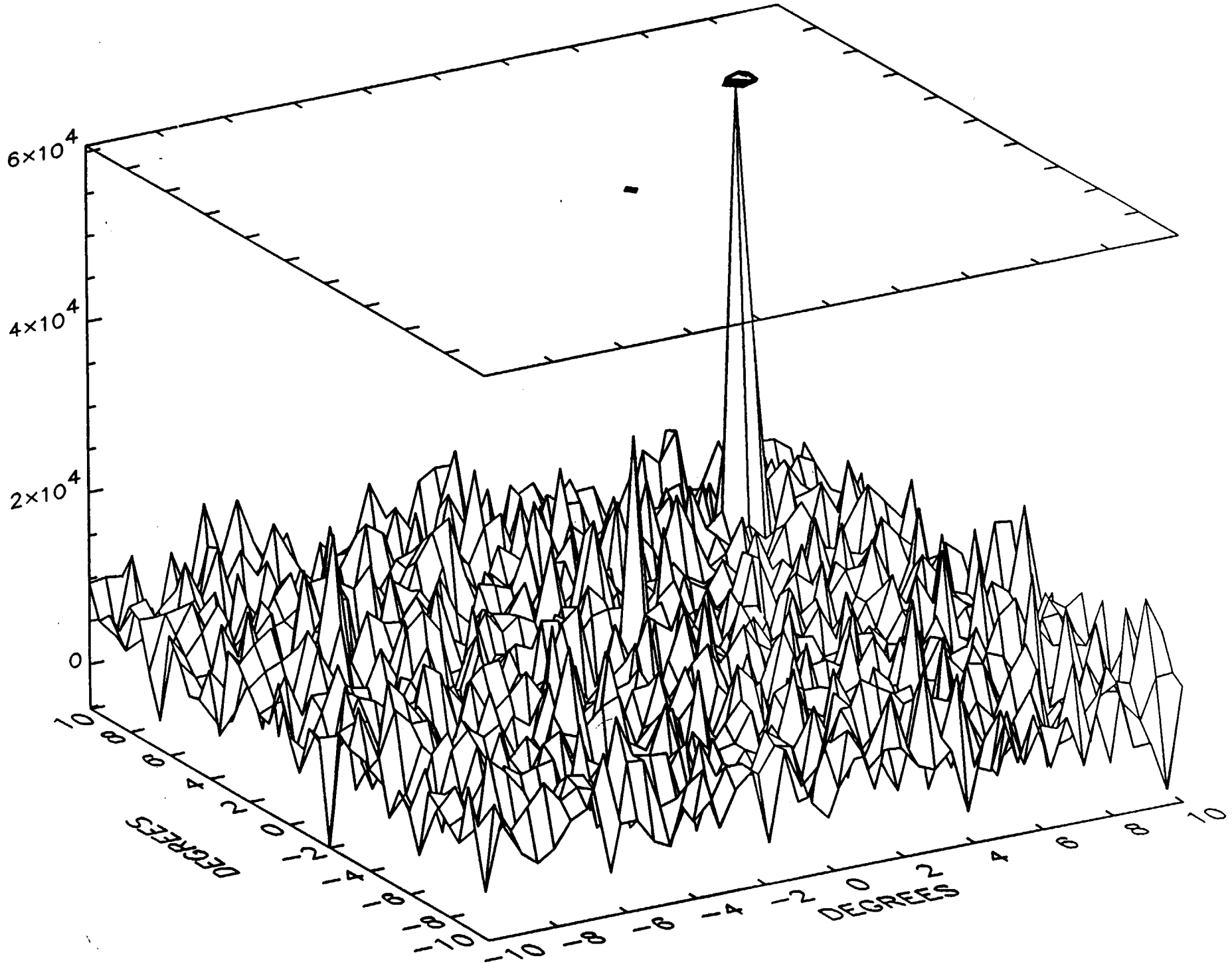
6×10^4
4×10^4
2×10^4
0
10
8
6
4
2
0
-2
-4
-6
-8
-10
DEGREES
-10 -8 -6 -4 -2 0 2 4 6 8 10
DEGREES

Fig. 8

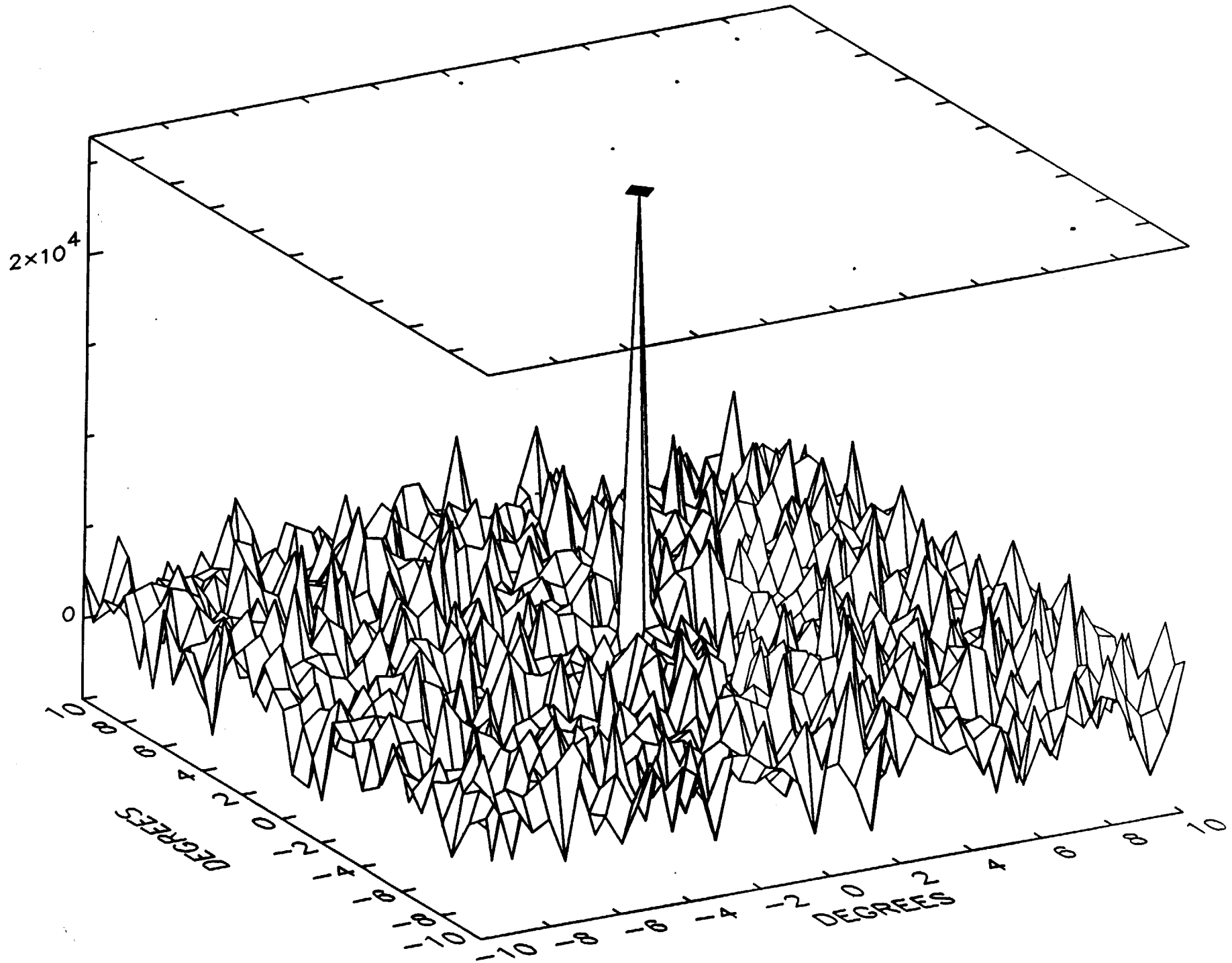

Fig. 9

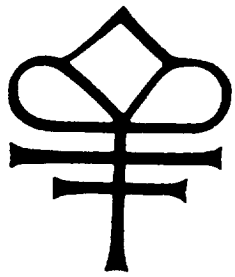

Appendix 2

THE IMAGING LIQUID XENON-CODED APERTURE TELESCOPE (LXe-CAT)

E. APRILE, A. BOLOTNIKOV, D. CHEN, H. TAWARA, & F. XU
Physics Department and Columbia Astrophysics Laboratory
538 West 120th Street, NY, NY 10027

E. CHUPP & P. DUNPHY
Physics Department and Inst. for the Study of Earth,
Oceans and Space (EOS)
University of New Hampshire, Durham, NH 03824

T. DOKE & J. KIKUCHI
Advanced Research Center for Science & Engineering
Waseda University, Tokyo 162 Japan

K. MASUDA
Physics Laboratory, Saitama College of Health
Saitama 338 Japan

G. FISHMAN & G. PENDLETON
NASA/Marshall Space Flight Center
Huntsville, AL 35812

To appear in: Experimental Astronomy
Proc. of the Workshop on *Imaging in High Energy Astrophysics*
Capri, 26 – 30 September 1994

COLUMBIA UNIVERSITY

DEPARTMENTS OF

PHYSICS and ASTRONOMY

NEW YORK, NEW YORK 10027

Columbia Astrophysics Laboratory Contribution Number 556

THE IMAGING LIQUID XENON-CODED APERTURE TELESCOPE (LXe-CAT)

E. APRILE, A. BOLOTNIKOV, D. CHEN, H. TAWARA, & F. XU
Physics Department and Columbia Astrophysics Laboratory
538 West 120th Street, NY, NY 10027

E. CHUPP & P. DUNPHY
Physics Department and Inst. for the Study of Earth,
Oceans and Space (EOS)
University of New Hampshire, Durham, NH 03824

T. DOKE & J. KIKUCHI
Advanced Research Center for Science & Engineering
Waseda University, Tokyo 162 Japan

K. MASUDA
Physics Laboratory, Saitama College of Health
Saitama 338 Japan

and

G. FISHMAN & G. PENDLETON
NASA/Marshall Space Flight Center
Huntsville, AL 35812

Abstract. We describe a unique γ-ray imaging telescope operating in the energy range 0.3–10 MeV. The basic element of the telescope is a liquid xenon time projection chamber (LXe-TPC) as γ-ray spectrometer and 3-D imager. Location and energy analysis of multiple Compton scattering events in the chamber will permit a reconstruction of the incoming γ-ray direction, thus allowing a significant reduction of background. A 10-liter LXe-TPC prototype, with 400 cm^2 active area and 5 cm drift gap has been built and is currently being tested with γ-ray sources in the laboratory. Initial results are presented. The combination of the LXe-TPC with a coded aperture (LXe-CAT), results in a telescope with superior detection efficiency, angular and energy resolution, and excellent background rejection capability. Simulation results on the instrument's ability to image the Crab Nebula region in a balloon observation are presented, as well as to image the 1.809 MeV ^{26}Al distribution from the Vela region, in a satellite observation.

Key words: γ-ray Astronomy – Imaging – Instrumentation

1. Instrument Description

The proposed telescope (Aprile et al. 1992a) combines a liquid xenon time projection chamber (LXe-TPC) as calorimeter and position sensitive γ-ray detector with a coded aperture mask to achieve precise measurement of the energy and angular distribution of γ-ray sources in the 0.3-10 MeV energy region (Fig. 1). The coded mask is a 43×41 element URA, with elements $0.81 \times 0.85 \times 1.2$ cm^3 in size. With a detector-mask separation of 100 cm, the angular "pixel" is $0.46° \times 0.48°$ over a $19.3° \times 19.3°$ FOV. The telescope point

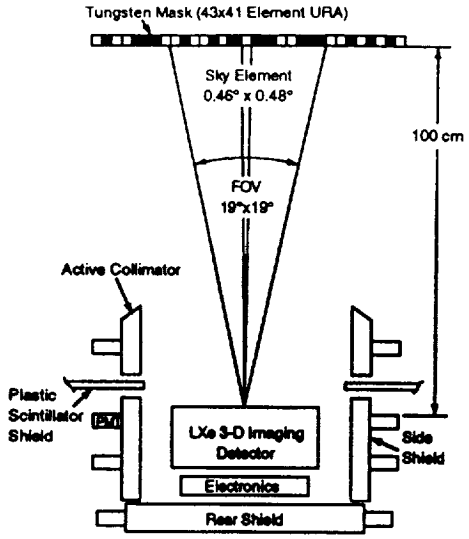

LXe-CAT Properties

Energy Range	0.3 - 10 MeV
Energy Resolution	5.9% FWHM at 1 MeV
3-D Spatial Resolution	< 1 mm
Geometrical Area	~1200 cm^2
Active Shield	5 cm CsI (or LXe)
FOV (Fully Coded)	19° x 19° FWHM
Angular Resolution	30 arcmin
Point Source	
Location Accuracy	~2 arcmin(10σ source)
Min Flux (Line)	8 x10^{-5} ph $cm^{-2}s^{-1}$
3σ at 1 MeV	(3 x 10^4s)
Min Flux (Continuum)	3 x 10^{-7} ph $cm^{-2}s^{-1}keV^{-1}$
3σ at 1 MeV	(3 x 10^4s)

Fig. 1 Schematic view of the Liquid Xenon-Coded Aperture Telescope (LXe-CAT)

source location accuracy is estimated at $2'$ for a $10\,\sigma$ source, due to the excellent signal-to-noise ratio of the imaging detector. The LXe-TPC has an active area of 1200 cm^2 and is surrounded by an active anticoincidence shield consisting of CsI or LXe scintillator. With a 10 cm deep layer of LXe ($Z = 54$, density = 3.06 g cm^{-3}), the full energy peak efficiency is about 65% at 1 MeV.

The LXe-TPC works on the principle that the free ionization electrons liberated by a γ-ray interaction in the liquid can drift, under a uniform electric field, toward a signal readout structure. The ionization signals induced on the readout sensing elements provide both the spatial and the total energy information for each event. In our design, the information in the $X - Y$ plane is obtained from the signals induced on two orthogonal wire planes, while the Z information, along the direction of drift, is inferred from the drift time, measured with respect to a time zero (see Fig. 2). The fast signal (< 10 ns) from the primary scintillation light of LXe, is used for time zero mesurement. With the capability of measuring the three spatial coordinates and the energy deposited for each γ-ray interaction, the TPC is therefore ideal for event reconstruction based on Compton kinematics. The direct outcome of this event visualization is the capability of background rejection for both single- and multiple-sites energy deposition events. This, as well as the polarization sensitivity of the LXe-TPC as Compton polarimeter, has been demonstrated with Monte Carlo simulation results (Aprile et al. 1993b, 1994a). The technical feasibility of such a detector and the factors which determine its ultimate energy and spatial resolution have been studied at Columbia for the past few years (Aprile et al. 1993a and references therein).

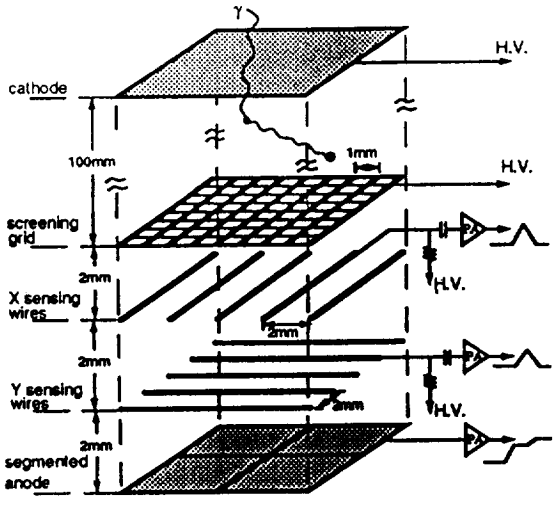

Fig. 2 Schematic view of electrodes system for 3-D position sensitivity of LXe-TPC

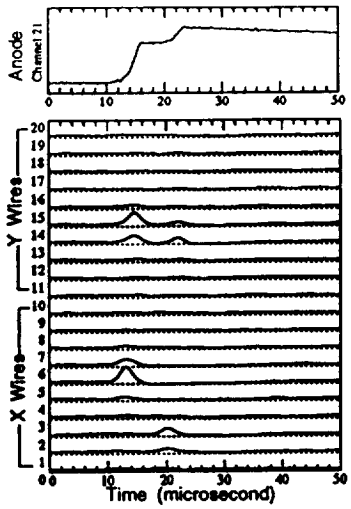

Fig. 3 On-line display of a Compton scattered γ-ray event (1.274MeV), showing the digitized waveforms induction signals and anode signal

2. Test Results with the 10-liter LXe-TPC Prototype Detector

To demonstrate the operation of a large liquid xenon detector, we have built and are currently testing a 10-liter LXe-TPC prototype, implemented with the electrode system shown in Fig. 2 (see Aprile et al. 1994b). With a wire spacing of 4 mm, the total number of sense wires for X-Y readout is 96. The prototype has half the drift gap, one third the sensitive area and a volume similar to that of the proposed flight instrument. Experiments have been carried out to test the instrument's spectroscopic and imaging performance. The detector's charge yield was as expected in high purity LXe and stable over a maximum period of 100 hr.

To simulate a parallel beam of γ-rays from a point source, a ^{60}Co or ^{22}Na source was placed 40 cm above the detector's sensitive area. Events with a single or multiple Compton scatterings, as well as photoabsorption events were accumulated. As an example, Figure 3 shows the on-line display of a 1.274 MeV γ-ray event from the ^{22}Na source experiment. The magnified view of the signal on the anode clearly shows a two-step event indicating that the γ-ray history was a Compton interaction followed by photoabsorption. The sum of the two steps pulse heights corresponds to 1.274 MeV total energy. From the amplitude and time analysis of the induction and collection signals, the coordinates and the energy for the two interaction points are inferred as well as their spatial separation. The most probable scattering angle can then be found from Compton scattering kinematics. These initial results directly demonstrate that the LXe-TPC can be very effective for background rejection based on Compton event reconstruction. In addition,

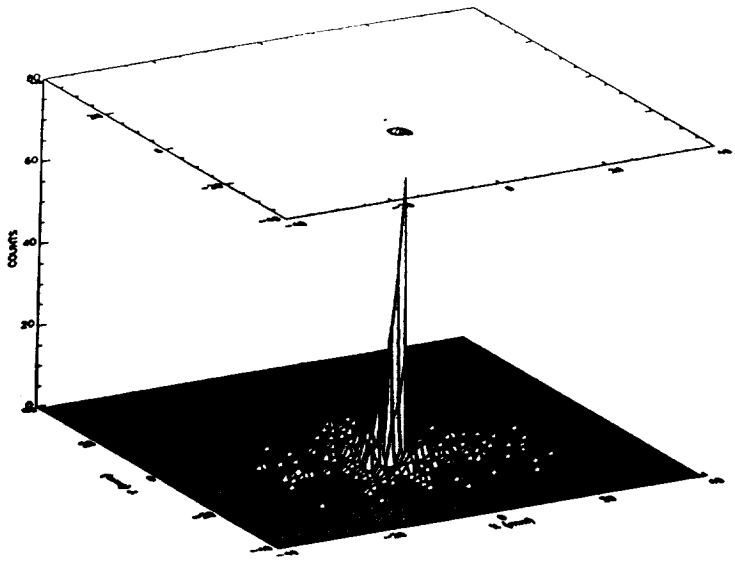

Fig. 4 2-D imaging of 662 keV γ-rays from collimated ^{137}Cs source (2 mm Ø collimation), detected with the 10 liter LXe-TPC

they verify that the original proposal (Aprile et al. 1989) to use a LXe-TPC as a Compton/pair telescope with large efficiency and good angular resolution is feasible for high energy γ-ray astronomy. As an indication of the detector's imaging performance, Fig. 4 shows the reconstructed image of a collimated beam (2 mm diameter collimator) of 662 keV γ-rays from a ^{137}Cs source. The data are consistent with a detector RMS spatial resolution of about 1 mm.

3. Simulation Results

To demonstrate the capability of the LXe-CAT as an imaging γ-ray telescope, we have carried out Monte Carlo calculations that simulate the response of the instrument to several source distributions. In particular, we simulate the imaging process for a coded aperture imaging system in response to photon continuum spectra from point sources and to a γ-ray line from localized sources. The background rates expected in a balloon or satellite based observation were calculated. Fig. 5 shows the total background spectrum, together with its individual components, calculated for 3 gcm^{-2} over Palestine, TX. A 5 cm CsI thick shield was assumed for the calculation.

To illustrate the response of the LXe-CAT to continuum spectra of γ-rays from discrete sources, we simulate the Crab Nebula for a typical balloon observation. The Crab spectrum is taken from Penningsfeld et al. 1979. The

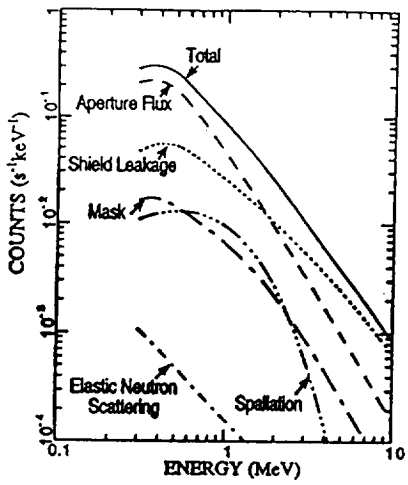

Fig. 5 Calculated background spectrum in LXe-CAT at 3 g cm^{-2} over Palestine, TX. A 5 cm thick CsI shield is assumed

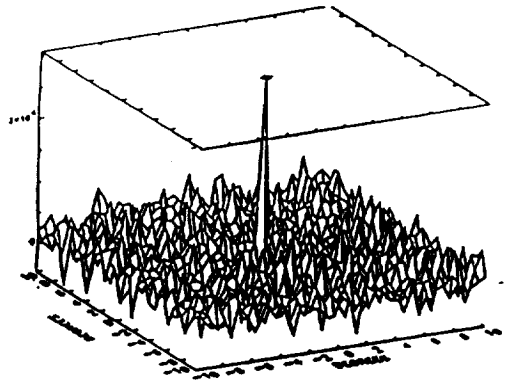

Fig. 6 Simulated image of Crab Nebula (0.5-1.0MeV) for 10 hr balloon observation

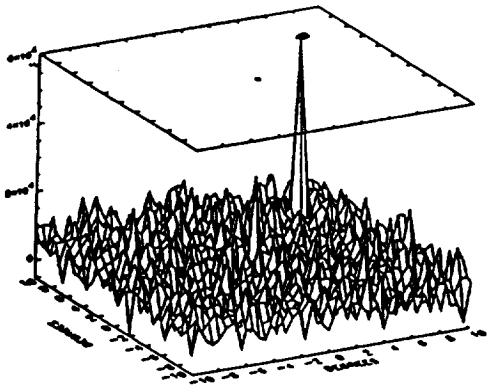

Fig. 7 Simulated image of Crab Nebula and quasar PKS 0528+134 (3-20MeV) for 336 hr satellite based observation

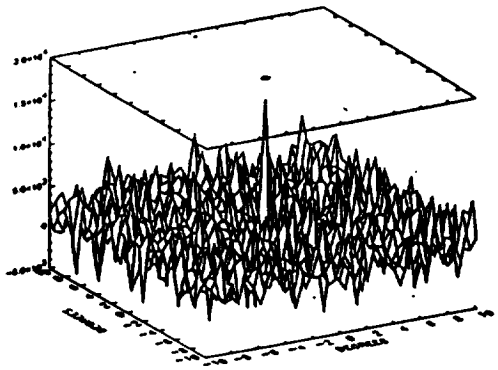

Fig. 8 Simulated image of Vela "hot spot" at 1.809MeV (^{26}Al) for an 8-week satellite-based observation

source observation time is taken to be 10 hours, with an equal length of time taken for measurement of background non-uniformity. The background rate of Fig. 5 was reduced by a factor of ~ 2 due to event rejection based on Compton reconstruction, but was increased by a factor of 2 as required by the evaluation of background non-uniformity. The source is present at a significance level of 16σ in the range 0.5–1 MeV (Fig. 6) and 11σ in the range 1–10 MeV. Since a point source can be located with a precision of $\sigma_{loc} = \sigma_{pixel}/n_\sigma$ (McConnell et al. 1987) and the characteristic size of a

pixel is about 30′, the uncertainty in the Crab Nebula location for this observation would be $\sim 2'$.

To illustrate the capability of the detector to resolve separate point sources in the same FOV, Fig. 7 shows the image for a satellite-based observation (336 hr) of the Crab Nebula and the quasar PKS 0528+134 (Collmar et al. 1993). The image of the quasar, in the energy range $3 - 20$ MeV, is seen at a significance level of $6\,\sigma$.

Finally, the measurement of the ^{26}Al distribution in the Galaxy via the 1.809 MeV γ-ray line is an important objective for γ-ray astronomy and for the LXe-CAT instrument (Aprile et al. 1994c). The maps of this radiation observed by *COMPTEL* (Diehl et al. 1994), show a highly structure emission over a wide longitude range with "hot spots" near the Galactic center the Vela region. Based on these maps, we have obtained the image shown in Fig. 8 for the Vela "hot spot." The result is for a satellite observation time of 1344 hr (similar to the *COMPTEL* observation time). The Vela "source," with a flux of $2.2 \times 10^{-5}\mathrm{cm}^{-2}\mathrm{s}^{-1}$, would have a significance of $9\,\sigma$ in the LXe-CAT.

This work was supported by a NASA Grant (NAGW-2013) to the Columbia Astrophysics Laboratory.

4. References

Aprile, E., Mukherjee, R., & Suzuki, M. 1989, SPIE Proc., 1159, 295.

Aprile, E., Bolotnikov, A., Chupp, E., & Dunphy, P. 1992, NASA proposal, CAL-2015.

Aprile, E., Bolotnikov, A., Chen, D., & Mukherjee, R., 1993a, Nucl. Phys. B. (Proc. Suppl.) 32, 279.

Aprile, E., Bolotnikov, A., Chen, D., & Mukherjee, R. 1993b, Nucl. Instr. and Meth. A327, 216.

Aprile, E., Bolotnikov, A., Chen, D., Mukherjee, R., & Xu, F. 1994a, ApJS, 92, 689.

Aprile, E., Bolotnikov, A., Chen, D., Muhkerjee, R., & Xu, F. 1994b, SPIE Proc. 2305, 33.

Aprile, E., Chupp, E., Bolotnikov, A., Dunphy, P., & Xu, F. 1994c, ApJ (submitted).

Collmar, W., et al. 1993, Proc. 23rd ICRC 1, 168.

Diehl, R., et al. 1994, AIP Conf. Proc., 304, ed. C. Fichtel, (AIP: NY) 147.

McConnell, M.L., Dunphy, P.P., Forrest, D.J., Chupp, E.L., & Owens, A. 1987, ApJ, 321, 543.

Penningsfeld, F.–P., Graser, U., & Schönfelder, V. 1979, Proc. 16th ICRC 1, 101.

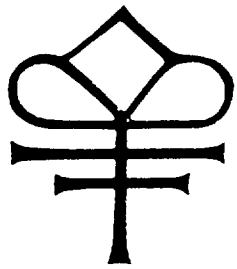

Appendix 3

Initial Results on Calorimetry and Imaging of

MeV γ-rays with a 10 Liter LXe-TPC

E. Aprile, A. Bolotnikov, D. Chen, H. Tawara, and F. Xu

Physics Department and Columbia Astrophysics Laboratory
Columbia University, New York, NY 10027

Presented at the: "Gamma-Ray Detector Physics and Applications"
Conference of the SPIE's International Symposium
on Optics, Imaging, and Instrumentation
24 – 29 July 1994

COLUMBIA UNIVERSITY

DEPARTMENTS OF

PHYSICS and ASTRONOMY

NEW YORK, NEW YORK 10027

Columbia Astrophysics Laboratory Contribution Number 549

Initial Results on Calorimetry and Imaging of MeV γ-rays with a 10 Liter LXe-TPC

E. Aprile, A. Bolotnikov, D. Chen, H. Tawara, and F. Xu

Physics Department and Columbia Astrophysics Laboratory
Columbia University, New York, NY 10027

ABSTRACT

The experiment LXe-CAT (Liquid Xenon-Coded Aperture Telescope), which we have proposed for γ-ray astrophysics observations in the 300 keV – 10 MeV energy range, uses a Liquid Xenon Time Projection Chamber (LXe-TPC) as a position sensitive γ-ray detector, and a coded aperture mask to provide a telescope with an angular resolution of 30′ over a Field-of-View (FOV) of 28° × 20°. The point source localization accuracy is about 2′ for a 10σ source.

To demonstrate the spectroscopy and imaging capabilities of the LXe-TPC as a γ-ray detector we have designed, built and are currently testing a 10 liter prototype with a sensitive area of $\sim$ 400 cm^2 and an active liquid depth of 5 cm. Studies on stability, spectroscopy and imaging response of this detector to various γ-ray sources will be presented. The unique capability of the LXe-TPC to identify and reject background events based on Compton kinematics reconstruction has also been demonstrated.

1. INTRODUCTION

The study of astrophysical γ-rays in the MeV region has always been challenging from an observational point of view, mainly due to the small source flux rate compared with the background rate, the small interaction cross-section and the complexity of Compton scattering which dominates in this energy range. Progress in MeV γ-ray astronomy relies on new telescopes with superior imaging capability, high energy resolution, wide sky coverage, and low background.

Two important astronomical observations which typify the need for novel imaging instruments are the 1.809 MeV line emission from radioactive ^{26}Al and the 0.511 MeV positron-electron annihilation line emission. The exact origin of these emissions is still undetermined. For both cases it is believed that a precise mapping of the spatial distribution of the emission will uniquely identify the origin of this γ-ray radiation based on the known distribution of the candidate sources[1].

Among the proposed novel techniques for imaging γ-ray sources in the MeV energy region, the LXe-TPC is recognized as very promising. The properties of LXe make it an excellent radiation detection medium for γ-rays. When used in an ionization chamber, operated in the time projection mode, LXe offers an ideal combination of high detection efficiency, three-dimensional (3-D) event imaging with submillimeter spatial resolution, and very good energy resolution response. Like an electronic bubble chamber, a TPC is capable of visualizing the complex histories of γ-ray events with multiple interactions, initiated by either Compton scattering or pair production. As a result of this imaging, efficient background rejection is also achieved, as well as sensitivity to γ-ray source polarization measurements.

To overcome the limited angular resolution of a LXe-TPC as a Compton telescope for MeV γ-rays,[2] we have proposed the LXe-CAT instrument, shown schematically in Fig. 1, for studies of galactic and extragalactic γ-ray sources in the energy range 0.3 – 10 MeV[3]. The telescope consists of a LXe-TPC as position sensitive detector, an active anticoincidence shield, to reduce the background rate at balloon altitude, and a coded mask. A list of the telescope's principal characteristics is also included in Fig. 1. The coded mask is a 2 × 2 mosaic of a basic uniformly

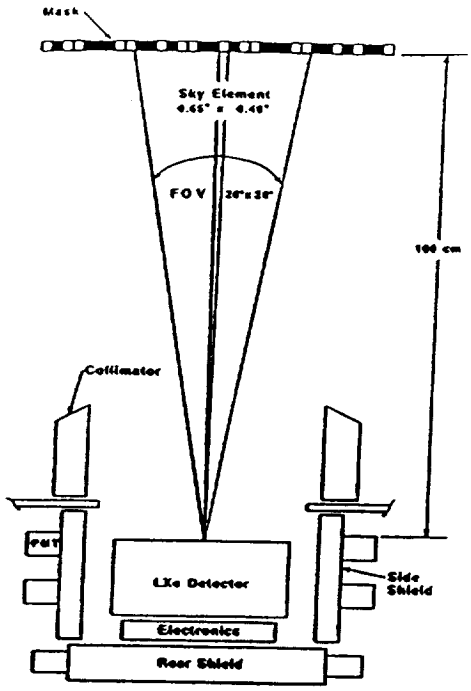

Energy Range	0.3-10 MeV
Energy Resolution	4.5% FWHM at 1 MeV
Spatial resolution	1 mm
Geometrical area	1200 cm^2
FOV (Fully Coded)	28° × 20° FWHM
Angular resolution	30′
Point source location accuracy	1′ (10σ source)
Min Flux (Line) 3σ at 1 MeV	8×10^{-5} ph $cm^{-2}s^{-1}$ (3×10^4s)
Min Flux (Continuum) 3σ at 1 MeV	3×10^{-7} ph $cm^{-2}s^{-1}keV^{-1}$ (3×10^4s)

Fig. 1 Schematic of the LXe-TPC/coded aperture imaging γ-ray telescope

redundant array (URA)[4]. It consists of a 43 × 41 element pattern of 0.91 × 0.68 × 1.2 cm^3 thick tungsten blocks. With a 1 m distance between the mask and the LXe detector plane, an angular pixel size of 0.65° × 0.49° and a FOV of 28° × 20° are defined. The active area of the LXe-TPC is 1200 cm^2 and the drift gap is 10 cm. With a thickness of 10 cm of LXe ($Z = 54$, density = 3.06 g/cm^3) the full energy peak efficiency at 1 MeV is about 35%, taking into account the presence of the mask. For a 10σ source strength, the point source localization accuracy is estimated to be 2′ based on the LXe detector spatial resolution of 1 mm rms.

The LXe-TPC works on the principle that the free ionization electrons liberated in the liquid by a γ-ray can drift, under a uniform electric field, toward a signal readout structure. The ionization signals induced on the readout sensing elements provide both the spatial and total energy information for each event. In our design the information in the $X - Y$ plane is obtained from the signals induced on two orthogonal wire planes, while the Z information, along the direction of drift, is inferred from the drift time, measured with respect to a time zero. The fast signal from the primary scintillation light of LXe, or the prompt ionization signal induced on a shielding grid can be used for time zero measurement. With the capability of measuring the three spatial coordinates and the energy deposited for each γ-ray interaction, the TPC is therefore ideal for event reconstruction based on Compton kinematics. The direct outcome of this event reconstruction is the capability of background rejection which is the most promising feature of this telescope. This, as well as the polarization sensitivity of the instrument, has been demonstrated with Monte Carlo simulation results[5,6].

The technical feasibility of such a detector has been studied at Columbia for the past few years[7–11]. A lot of work has been carried out on the key areas of: 1) achieving and maintaining the required liquid purity for a large volume detector; 2) triggering capability of the scintillation light signal; 3) energy resolution studies; 4) 3-D position

sensitivity based on a non-destructive signal readout. The results obtained give us the confidence in the performance of LXe γ-ray detectors and their applications in astrophysics. In order to demonstrate the direct imaging capability of a large volume LXe-TPC, we have designed and built a 10 liter prototype, which has about one third of the sensitive area planned for the balloon flight instrument. The detector is currently being tested for its cryogenic, spectroscopy and imaging performance. Here we will discuss the design philosophy and describe in details this TPC system, including the cryogenics, inner readout structure, and electronics system. The initial experimental results obtained with this large prototype are also presented here.

2. LXe-TPC 10 LITER PROTOTYPE

2.1. Xenon Purification System

The purity of the LXe is an essential requirement for the operation of the proposed LXe-TPC. Fig. 2 shows the schematic of the purification and gas handling system which has been built and used for filling the large volume TPC. It uses commercially available purifiers and only UHV components. The purified gas is stored in two stainless steel high pressure cylinders which are also used to recover the gas from the TPC after each experiment. We have already demonstrated that a sequence of Oxisorb[12], cold molecular sieves and high temperature getter is capable of purifying the xenon gas to the sub-ppb level. This purity level is needed to drift ionization electrons over large distances[7].

A gridded ionization chamber can be used to monitor the purity of the liquid xenon by detecting the signals of cosmic rays traversing the detection volume. The measurement is usually done at very low electric field strength to achieve long drift time, in order to get better sensitivity to the effect of electron attachment by electronegative impurities. From a pulse shape analysis of the signals induced on the anode by the drifting electrons, information on the electron lifetime and thus on the total impurity concentration can be obtained.

Fig. 3 is a typical cosmic ray signal registered in a 3.5 liter gridded ionization chamber used as purity monitor. A linearly rising signal with a long rise time is a direct indication of good liquid purity. An electron lifetime, longer than 1 msec in LXe, has been achieved. It indicates an impurity level of < 1 ppb O_2 equivalent. This purity level is more than sufficient for our proposed detector where the maximum drift time is not longer than 40 μsec.

2.2. Chamber and Cryostat

The 10 liter LXe-TPC consists of an inner cylindrical vessel, in which we fill the ultra-pure LXe and mount the electrode structure, surrounded by an external vessel which is used as a cryostat. Both vessels are made of stainless steel. Fig. 4 shows the cross-section of the system. The volume between the two vessels is evacuated and maintained at a pressure of $10^{-5} \sim 10^{-6}$ Torr. To achieve better thermal insulation, a few layers of aluminized Mylar foil are used to surround the inner vessel. The inner vessel is constructed with standard UHV technique. All the construction materials are bakeable and capable of working at cryogenic temperature. This inner vessel is designed to withstand a pressure up to 5 atm. The normal operating pressure is around 1.5 atm. The inner vessel bottom is a 16-1/2″ bolted flange, on which the whole electrode structure is supported.

The cooling of the TPC is achieved by a controlled flow of LN_2, through the copper coil of the condenser provided on top of the inner vessel. The coil has 1/4″ diameter and $\sim$ 15″ effective length. The condenser is thermally insulated by a vacuum jacket up to the top, where the port for pumping and gas filling is located. During the operation of the system, the vapor pressure on top of the liquid is monitored by a pressure gauge and controlled by the LN_2 flow in the condenser.

It has been tested that such a cooling system is very effective and efficient. It needs about 80 liters of LN_2 and 4 hours to fill the 10 liter chamber, and about 5 liters of LN_2 every 3 hours to keep the operating condition.

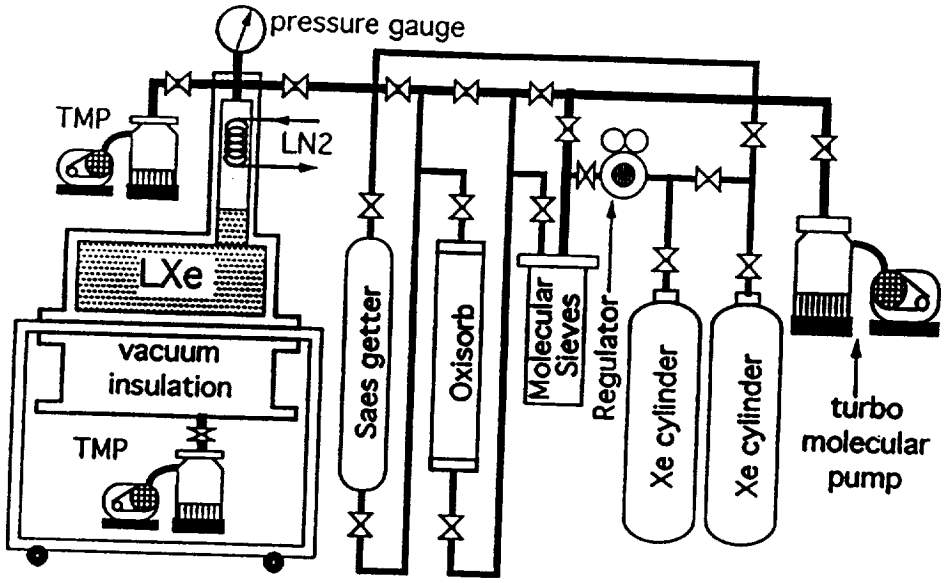

Fig. 2 Schematic of the xenon gas purification and handling system

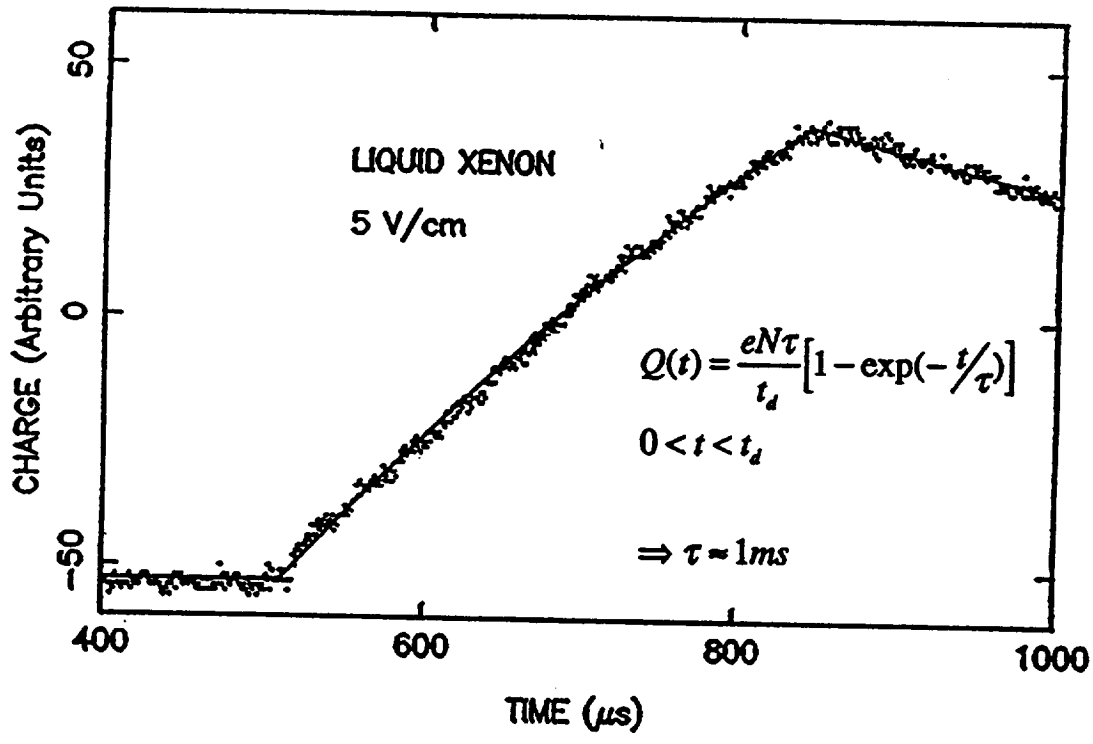

Fig. 3 Typical cosmic ray signal detected in a 3.5 liter gridded ionization chamber at a drift field of 5 V/cm

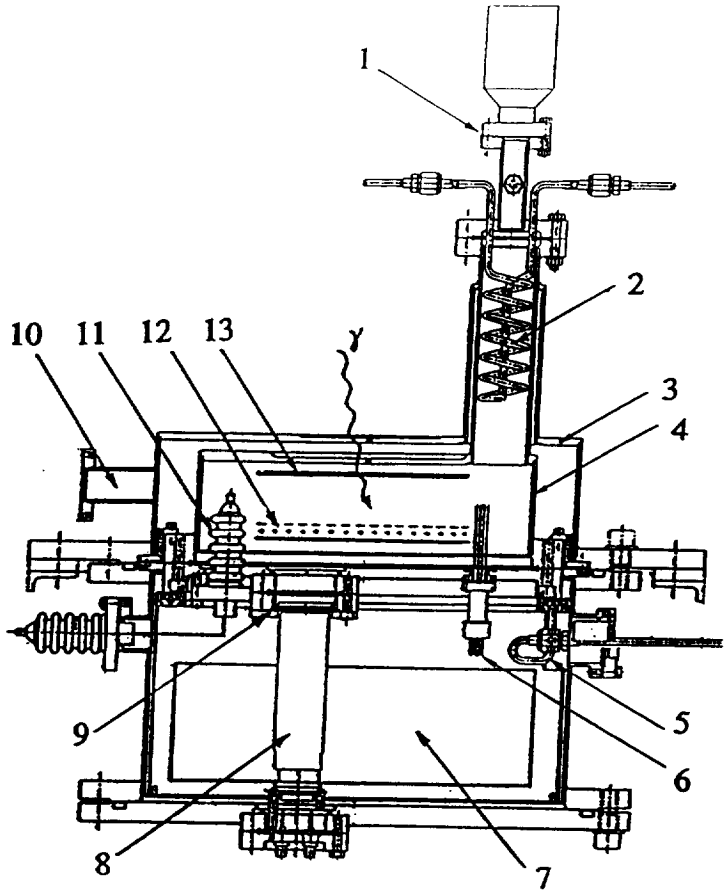

Fig. 4 Schematic of the 10 liter LXe-TPC prototype
1—gas inlet, pumping and pressure gauge; 2—condenser; 3—outer vessel; 4—inner vessel;
5—cooling coil for electronics; 6—multipin feedthroughs; 7—preamplifier boxes; 8—UV PMTs;
9—quartz windows; 10—cryostat pumping; 11—HV feedthroughs; 12—readout structure; 13—cathode

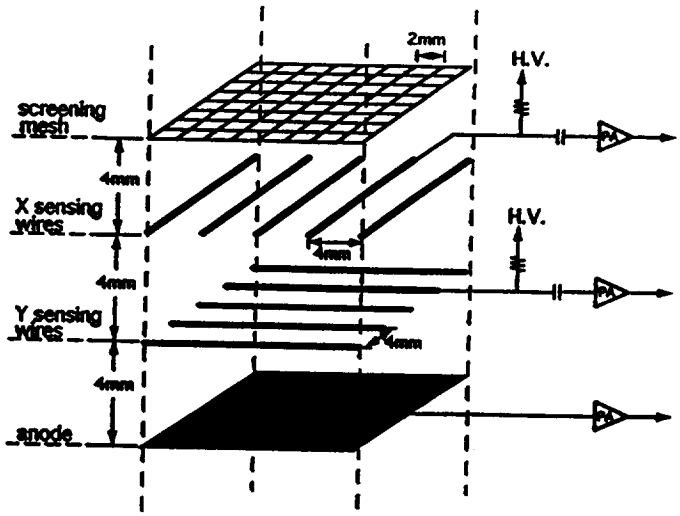

Fig. 5. Schematic of inner electrode structure for 10 LXe-TPC prototype

Two UV transparent windows on the inner bottom flange are optional for detecting the primary scintillation light with UV sensitive photomultipliers. Crystal quartz is chosen for its high transmission at the wavelength of 175 nm of the xenon scintillation light.

2.3. Electrode Structure

For imaging the point-like charge blobs produced by MeV γ-rays in LXe, we have proposed the non-destructive readout structure[11], schematically shown in Fig. 5. It consists of two orthogonal induction wire planes, followed by a plate anode for total energy measurement. The plate anode can be segmented into sections, each connected to its own charge sensitive amplifier, to reduce the input capacitance and hence the electronic noise. A shielding grid separates the sensing region from the drift region. A point-like charge produced within the sensitive volume and drifting to the wire planes has to pass through the shielding grid and the induction planes without loss, to be fully collected on the anode. This is achieved by choosing the proper electric field ratio before and after these planes. As soon as the ionization electrons are created and start moving in the drift region, they will induce a current pulse on the grid, which is a function of drifting distance and can be used to indicate the initial position where the charge was produced. Once passed through the grid, the electrons induce a positive current on the wires below, when they are approaching, and a negative current, when they are drifting away from the wires. Fig. 6 shows the current and charge signal waveforms on the grid, induction wire and anode produced by a point-like charge. While the induction signal is triangular in shape, the collection signal from the anode plate is step-like. The signals induced on the wires provide the $X-Y$ coordinate information. The measured drift time, referred to a time zero, together with the known drift velocity, provides the Z-coordinate information. For γ-ray events with multiple Compton interactions, the height of each step in the resulting anode signal gives the energy deposited in each point, and the time interval between each step gives the relative distance of the interaction points, along the drift direction. The sum of all the step pulse heights is proportional to the total energy of the original γ-ray, if totally absorbed. When combined with the additional $X-Y$ information inferred from the induction signals, 3-D imaging and calorimetry is achieved for each event.

This readout structure also permits to improve the accuracy of the $X-Y$ information, by using the point-like ionization feature produced by low energy γ-rays in LXe. In fact, the amplitude of the signal induced by a point-like charge blob depends strongly on its initial lateral position with respect to the sensing wire. This position dependence allows to derive the spatial coordinate of each blob by weighting the signal amplitudes on neighboring wires. Thus the spatial resolution in the detector plane can be better than the wire spacing, and is determined by the accuracy of the amplitude measurement, i.e. the signal-to-noise ratio. Ultimately, the localization of a charge blob is limited by its physical extension and its diffusion during the drift. For a 1 MeV electron in LXe, the intrinsic size of the charge blob is on the order of 0.5 mm. The lateral diffusion, orthogonal to the drift direction, is given by $\sqrt{Dt_d}$, where $D = 65$ cm^{2}s^{-1} is the diffusion coefficient[13], t_d is the drift time. For a maximum drift time of 40 μsec, as in the proposed LXe-TPC, the resulting value is about 0.5 mm.

This readout scheme has been implemented and tested with the 10 liter LXe-TPC prototype. Initial tests have been made with a 3 cm drift gap, to minimize the applied voltages on the grid and induction wires.

The sensitive area of the anode is 19 cm x 19 cm. It is segmented into four identical 9 cm x 9 cm squares, each coupled to its own preamplifier. The sensitive volume is thus only 1,200 cm^3. The total liquid volume of 10 liters is however of the same order as the sensitive volume of the proposed flight instrument.

The shielding grid is a mesh made of 100 μm diameter stainless steel wires with a pitch of 2 μm, orthogonally stretched on the same ceramic bars on which the induction wires are stretched, to allow for good alignment and therefore minimum electron trapping. The sense wires are also made of 100 μm diameter stainless steel wires, with 4 mm pitch for both X and Y readout. The gap between the different layers is also 4 mm. The mesh in this arrangement has a shielding inefficiency of about 3%, according to the Bunemann's formula[14], modified for 2-dimensional grid. The fields above (E_1) and below (E_2) the shielding grid are chosen to permit complete transparency to the drifting electrons. Here, a field ratio E_2/E_1 larger or equal to two is used for 100% transmission.

The assembled electrodes structure is mounted on the bottom flange. HV is separately provided to the cathode

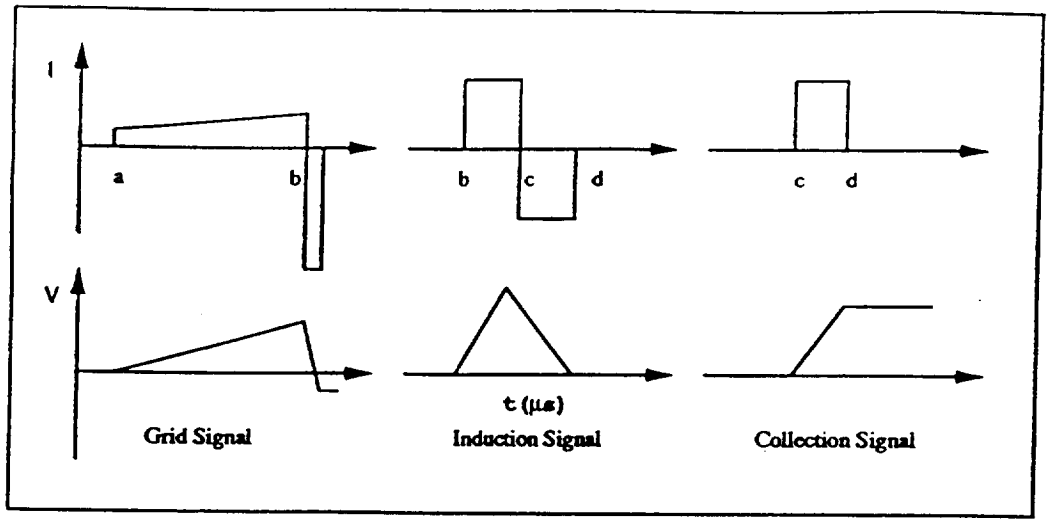

Fig. 6 Signal waveforms on grid, induction wire and anode plate: a) initial charge position, b) grid wire, c) induction wire, d) anode plate

and the grid. Commercially available multi-pin feedthroughs (10 pins each, rated for 3.3 kV), also mounted on the bottom flange, are used for the induction signals.

2.4. Front-End Electronics

The requirements for the front-end electronics include low noise, low power consumption, and compactness. The ionization produced by 1 MeV radiation in LXe corresponds to $\sim 60,000\ e^-$. At a drift field of 1 kV/cm, only $\sim 80\%$ of these electrons are collected. In order to view events with multiple Compton interactions, the $X-Y$ wires should be able to sense point-like charge blobs with a minimum energy deposition of 100 keV, or 5,000 e^- in LXe. In addition, the signal on the induction wire is less than the total charge and depends on the lateral distance from the charge blob to the wire. To obtain a reasonable S/N ratio, the noise from the preamplifier, with the HV applied, has to be reduced to a level of $\sim 1,000\ e^-$ rms or better.

The total number of sense wires for the multiwire readout structure under test is 96. Each sense wire is connected to a low noise charge sensitive hybrid FET preamplifier via a high voltage capacitor, to decouple the input from the applied voltage on the wire. The signal decay time constant is 220 μsec for the induction wires and 1 msec for the anodes. All the preamplifiers are enclosed in the cryostat which provides a perfect shielding as a Faraday cage. The power consumption of the preamplifiers should be as low as possible, given the power limitations imposed by a balloon flight experiment. The low power dissipation is also important to avoid the bubbling of the liquid, and hence the low frequency noise, due to heat transfer via thermal conduction and thermal radiation.

With a bias of $\pm$6V the present hybrids dissipate 50 mW/channel. The noise level, with the preamplifier connected to the wire is about 400 e^- rms, and slightly larger with the HV on the electrodes.

The preamplifier outputs are brought outside the cryostat through multipin connectors mounted on the wall of the cryostat, and given to the second stage amplifiers via shielded twisted-pair cables for filtering and further amplification needed by the waveform digitizers. The shielded twisted pair cable can effectively avoid noise pick-up and cross-talk between channels.

2.5. Signal Triggering and Data Acquisition

To test the imaging performance of the 10 liter LXe-TPC, γ-ray data have been taken with the detector in a self-triggering mode, using the charge collection information recorded on the anode with external calibrated γ-ray sources. In order to insure that the incoming γ-ray energy is totally contained within the sensitive volume, we select an energy window around the full energy peak of the source spectrum. As shown in Fig. 7, the ionization signal from the anode is digitized, after proper amplification, as well as used for event triggering. To be used for triggering, the anode signal is passed through a shaping amplifier before being fed into a single channel analyzer which generates a logic gate signal whenever the pulse height corresponds to the selected full-energy peak. This logic signal, after proper delay, is used as a common stop for the CAMAC based LeCroy 2262 FADC system.

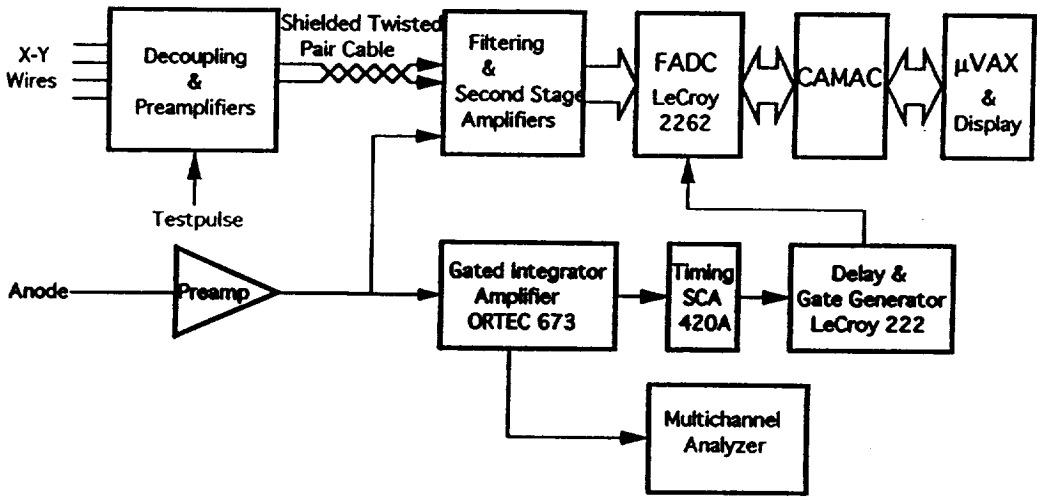

Fig. 7 Block diagram of front-end electronics and data acquisition system

A distinguished feature of LeCroy 2262 FADC is its post-triggering capability. This is needed for the present set-up, since the anode signal is detected later in time than the induction signal on the wires. The FADC has a 10 bit resolution and a sampling period of 200 ns, which corresponds to 320 sampling points over a period of 64 μsec.

The digitized anode and induction wires waveforms for each γ-ray event are transferred to a μVAX for online display and offline analysis.

The TPC spectral response is directly measured from the anode signal, using a multichannel analyzer (MCA). The anode signal is first amplified and shaped with a research amplifier or a gated integrator[11].

3. EXPERIMENTAL RESULTS AND DISCUSSIONS

We have carried out repeated experiments with the 10 liter LXe-TPC prototype and have achieved the primary design objectives: (1) verify that the 10 liters of liquid xenon can be purified and kept clean for good charge collection over a period of several days; (2) demonstrate simultaneous spectroscopy and imaging of MeV γ-rays, with good

energy resolution and submillimeter spatial resolution; (3) use the measured energy and spatial information for event reconstruction by Compton kinematics and identification of the first Compton interaction point.

In the following, we summarize the experimental results achieved so far. For the imaging performance, only 20 of the induction wires were used, due to the available number of second stage amplifiers and digitizers.

3.1. System Stability

The long term stability of the LXe-TPC performance has been monitored for a running time of four days. The full-energy peak position of the 511 keV γ-rays from a ^{22}Na source was used as an indicator of the charge stability as a function of time. Results are shown in Fig. 8, indicating no appreciable decrease in charge collection over the entire period of the run. The collected charge is consistent with the result expected with good liquid purity. The fluctuation around the straight line fit is attributed to the error in peak position reading from different measurements and to the stability of the electronics and the high voltage power supply. A better control of the operating conditions should reduce this fluctuation.

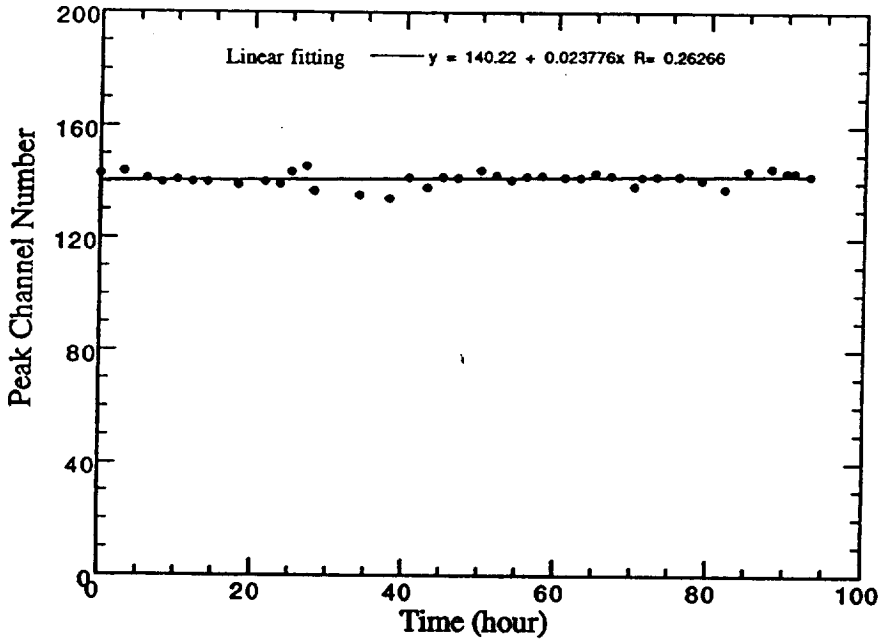

Fig. 8 Charge collection yield from 511 keV γ-ray as a function of time, obtained with 10 liter LXe-TPC at a drift field of 1 kV/cm

3.2. Spectroscopy Performance

The energy response was measured with collimated ^{137}Cs and ^{22}Na γ-ray sources as a function of applied electric field in the range of $0.5 \sim 1.75 kV/cm$. Typical pulse height spectra are shown in Fig. 9 for a drift field of 1 kV/cm.

The spectra were obtained with a MCA after a 6 μsec gated integrator shaping time. The rightmost peak is the test pulse distribution, indicating an electronics noise contribution of about 400 e^- rms, or 20 keV FWHM.

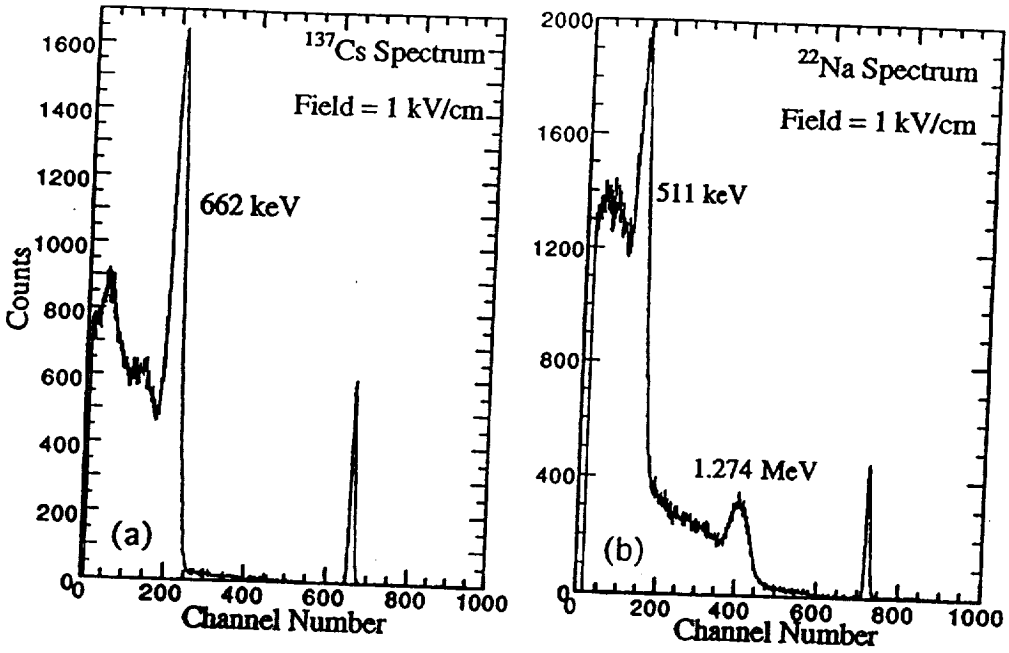

Fig. 9 (a) ^{137}Cs and (b) ^{22}Na spectra obtained with 10 liter LXe-TPC at a drift field of 1 kV/cm

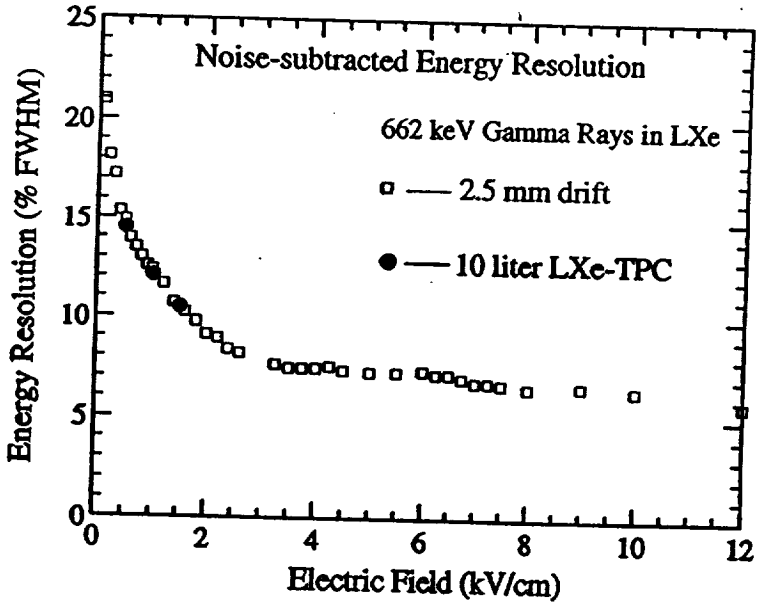

Fig. 10 Comparison of FWHM energy resolution with (•)10 liter LXe-TPC and (□) small volume gridded ionization chamber [5]

In Fig. 10, the energy resolution obtained with the 10 liter LXe-TPC is compared with that previously measured with simple gridded ionization chambers of much smaller volume and only a few millimeters of drift gap[9]. The open squares are the 570 keV FWHM energy resolution data, normalized to 662 keV by the $E^{-1/2}$ law. The closed circles are the data from the 10 liter LXe-TPC irradiated with ^{137}Cs. The noise-subtracted energy resolution is 12.1% FWHM at 662 keV, comparable to that in the much smaller chamber, at the same drift field of 1 kV/cm. This implies that the liquid purity is sufficient for long drift and the signal processing with the gated integrator prevents the resolution from degradation due to the ballistic deficit as discussed in ref. 11.

These results are very encouraging. Better energy resolution can be achieved at higher drift fields, by reducing the effect of charge loss in electron-ion recombination. For example, at 4 kV/cm we have measured a resolution of 7% FWHM for 662 keV γ-rays with a 3.5 liter gridded chamber and 5 cm drift gap [16]. However, in the TPC mode of operation, the detection of small induced signals in presense of HV, makes this approach difficult. A more practical approach is provided by the photoionization effect in LXe doped with appropriate organic molecules, to convert the scintillation light to charge. The increased charge collection and reduced fluctuation in recombination results in improved energy resolution[15]. We started our studies in this direction with LXe doped with TMA (trimethylamine), which is believed to be the most efficient photoconverter with LXe. We have tested the spectroscopy response of LXe-TMA with a gridded ionization chamber of 1 liter volume.

Fig. 11 shows the system used for the doping experiments. Xenon gas is purified by an Oxisorb followed by a spark purification chamber [17]. TMA is purified separately with vacuum distillation and trapping with cold molecular sieves. The test chamber includes a UV sapphire window to couple a PMT to the sensitive volume and study the quenching of the light by the dopant. We have observed encouraging spectral improvement with even a small concentration of TMA (7.5 ppm). Fig. 12 shows the spectra of ^{207}Bi obtained in pure xenon and doped xenon at same electric field of 5 kV/cm. The better separation of the two higher energy lines (976 keV conversion electron and 1048 keV γ-ray) can be clearly seen in the spectrum with doped xenon. In Fig. 13, the lower curve is the field dependence of the energy resolution in LXe with 7.5 ppm TMA, while the upper curve is obtained with pure LXe. To test the stability of the detector's response with time, we operated the chamber for more than 7 hours. No appreciable change in charge collection was observed (see Fig. 14). We will continue these experiments with different concentrations of TMA to find the optimum in energy resolution and system stability.

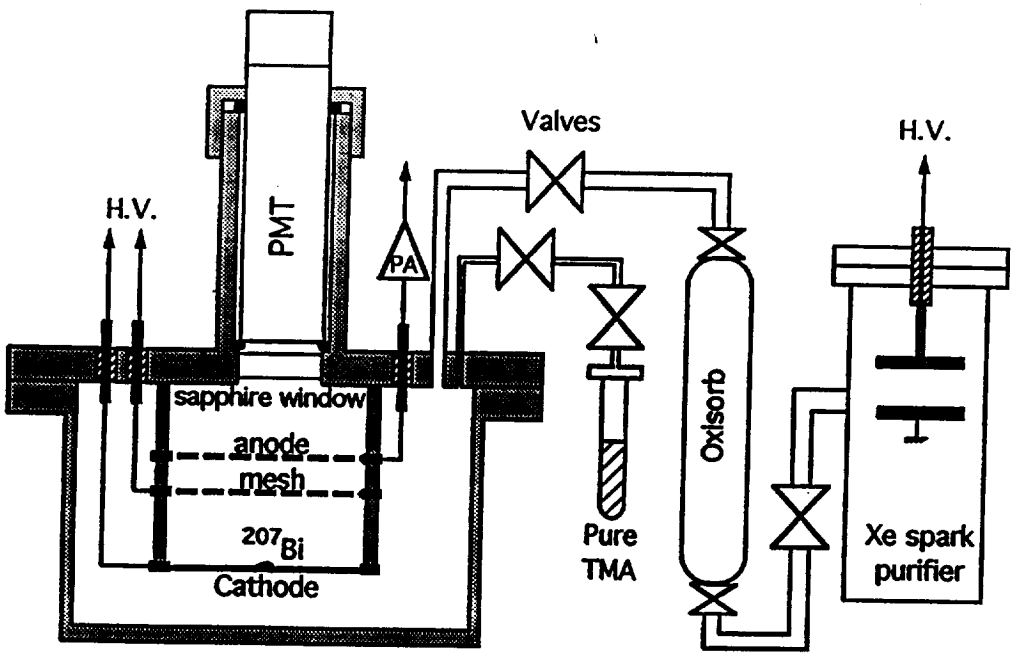

Fig. 11 Test chamber and purification system for studies with TMA doped LXe

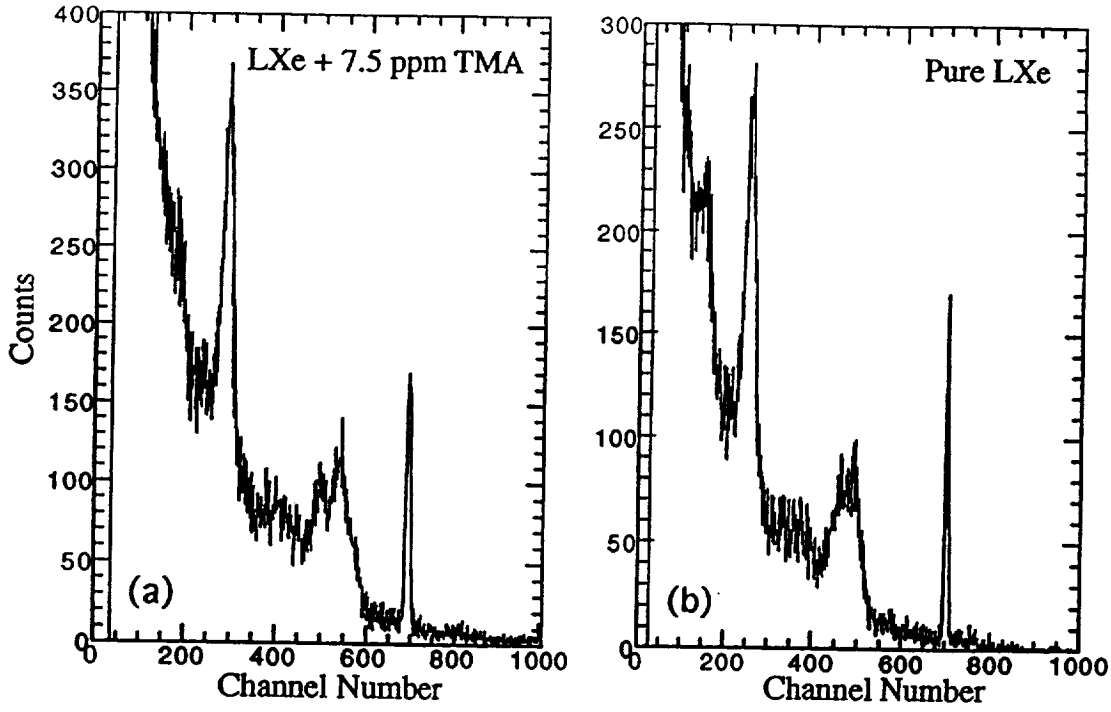

Fig. 12 Comparison of ^{207}Bi spectra obtained with (a) TMA doped LXe (b) pure LXe at the same drift field of 5 kV/cm

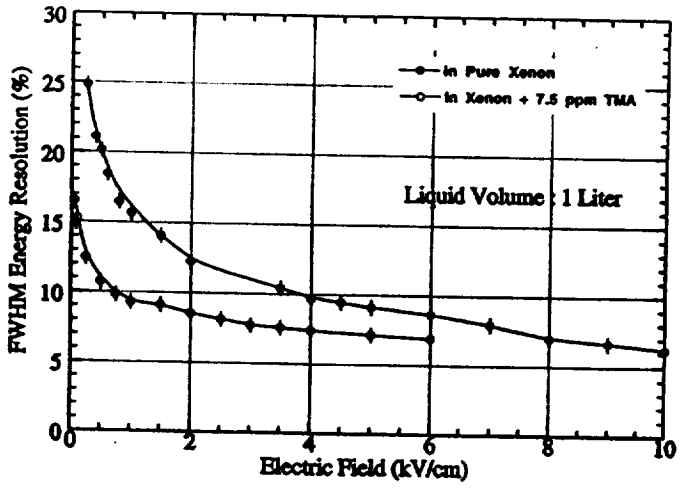

Fig. 13 Field dependence of FWHM energy resolution for 570 keV γ-ray in (o) pure LXe and (•) LXe doped with 7.5 ppm TMA

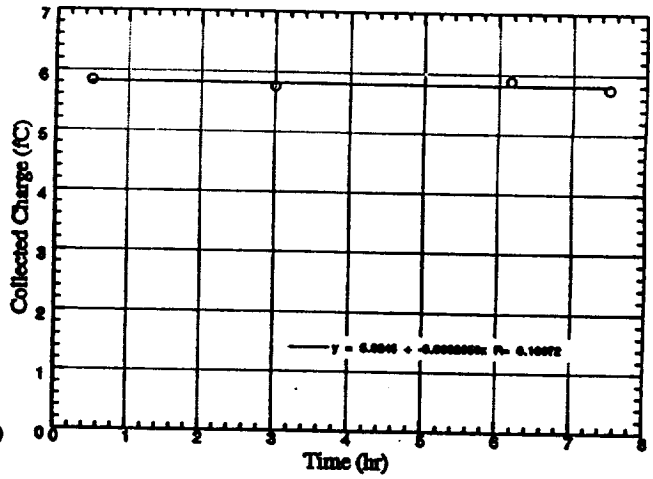

Fig. 14 Collected charge as a function of time for 570 keV γ-ray interaction inside LXe doped with 7.5 ppm TMA

3.3. Imaging Performance

Due to the limited number of readout electronic channels, we used only part of the readout structure (10 X-wires, 10 Y-wires, and the corresponding section of the anode plate located below these sense wires, corresponding to a sensitive area of 4 cm × 4 cm) to obtain the spectrum and imaging of a collimated γ-ray beam from ^{137}Cs. The collimator is made with two lead blocks with a thickness of 5 cm and a hole of 2 mm diameter.

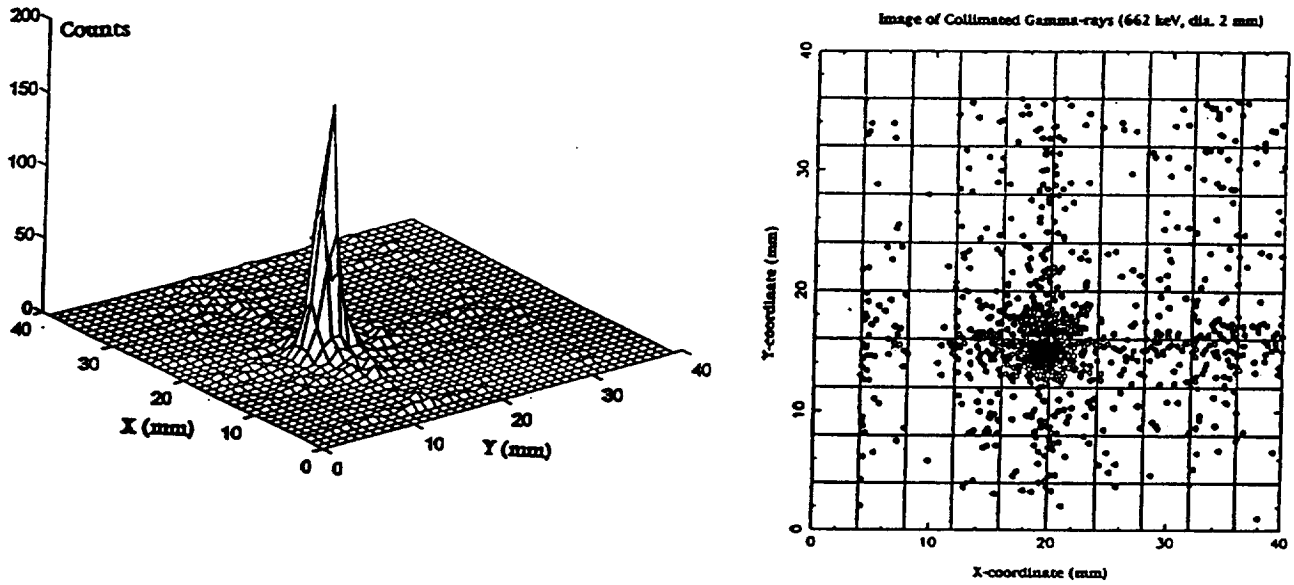

Fig. 15 2-D distribution of ~2000 events of 662 keV γ-rays from collimated ^{137}Cs source detected with the 10 liter LXe-TPC. The diameter of the collimator is 2 mm.

By weighting the signals induced on two neighboring sense wires by a charge blob produced by a γ-ray, one can locate the interaction point coordinates in the $X-Y$ plane with a precision much better than the 4 mm wire spacing. Triggering on 662 keV γ-rays from the full-energy peak, the collimated 2 mm diameter beam was imaged by this readout structure. Fig. 15 shows the 2-D image of this vertically incident beam. The beam width is measured as $\sigma = 1.6$ mm, including the possible spread due to the solid angle effect of the collimation, the inclination of the beam, as well as the spread due to Compton scattering. The centroid finding algorithm used for this analysis needs to be optimized. More data have been accumulated and we expect that a cleaner image with less background will be obtained.

The preliminary imaging results of Fig. 15 together with the good energy resolution shown in Fig. 10, obtained simultaneously, represents the realization of the second design objective of this LXe-TPC development.

3.4. Compton Kinematics and Event Reconstruction

It is another design objective and a unique capability of the LXe-TPC to identify the first Compton interaction

point and to reconstruct the incident γ-ray direction by means of Compton kinematics. The former is required by the coded aperture imaging and the latter is needed to identify and reject background. The following example demonstrates how the measured energy and spatial information for a Compton scattering event is used to reconstruct its topology. Combining the induction signals on the $X-Y$ plane with the collection signal on the anode, the (X, Y, Z) coordinates as well as the energy deposition E at the scattering and absorption points can be obtained. With this information, Compton kinematics can be used to find if the incident γ-ray direction is within the FOV. Fig. 16 is the on-line display of a ^{60}Co γ-ray event, showing the digitized signals from the 10 X-wire, 10 Y-wires and the anode. The source was placed 10 cm above the 4 cm x 4 cm sensitive area of the detector, to approximate a celestial γ-ray point source. The event was recorded with the trigger from the 1.33 MeV full energy peak of ^{60}Co. Channel $1 \sim 10$ correspond to the X-wires, $11 \sim 19$ to the Y-wires and channel 20 corresponds to the anode waveform. The zoom view of channel 20 clearly shows a 2-step pulse shape. The amplitude of the steps is proportional to the energy deposited in the two interaction points, their sum corresponding to the total energy of 1.33 MeV. The time interval between the two steps gives the vertical separation Z of the two interaction points, given the known drift velocity at 1 kV/cm. Each step has its corresponding induction pulses on two neighboring X-wires and two Y-wires, respectively.

We define the coordinates of channel 1 and channel 11 as the origin of the $X-Y$ plane ($X=0$ and $Y=0$, respectively), and the first charge blob in time is at $Z=0$. From the analysis of the waveforms in Figure 14, the two charge blobs (A and B) have coordinates and energy depositions as follows:

	X (mm)	Y (mm)	Z (mm)	E (MeV)
Blob A	20.1	23.2	0.0	0.60
Blob B	28.0	28.0	8.0	0.73

where, Z was inferred from the drift time interval between two steps in anode signal, X and Y coordinates were obtained by weighting the amplitudes of the induced signals, and E is the energy deposition at the interaction site, proportional to the step height over the total pulse height. These quantities are precise extracted from the waveforms through off-line data analysis.

Fig. 17 shows the reconstructed event in 3-D space. The most probable incident direction is vertically down along the Z direction. From geometry, the angle θ_g is 49°, obtained from $\tan\theta_g = l/Z$, where l is the lateral separation between the two charge blobs. The Compton scattering angle, θ_c, can be compared to θ_g to directly identify the first interaction point.

$$1 - cos\theta_c = \frac{0.511MeV}{E_2} - \frac{0.511MeV}{E_0}$$

where $E_0 = E_1 + E_2 = 1.33$ MeV, the energy of the incoming γ-ray. If the scattered photon has energy $E_2 = 0.60$ MeV, then $\theta_c = 58°$, and Compton kinematics is not satisfied. If the scattered photon has energy $E_2 = 0.73$ MeV, we obtain $\theta_c = 47°$. The match between the geometry measurement and Compton kinematics identifies point A as the first Compton interaction point and the event as a case of forward scattering.

This Compton event identification procedure can be generally done with a reconstruction algorithm based on Compton kinematics[5]. Following the formalism of ref. 5, we define the function f as:

$$f = \sum_{i=0}^{N-1} (W_i - W_i')^2$$

where W_i is the energy of the ith scattered photon calculated from the Compton formula, while W_i' is the energy of the same scattered photon but derived from energy conservation only. To test the validity of the assumption that the total energy is contained, as well as if the assumed initial direction of the γ-ray is kinematically possible, this function is minimized for all possible combination of points.

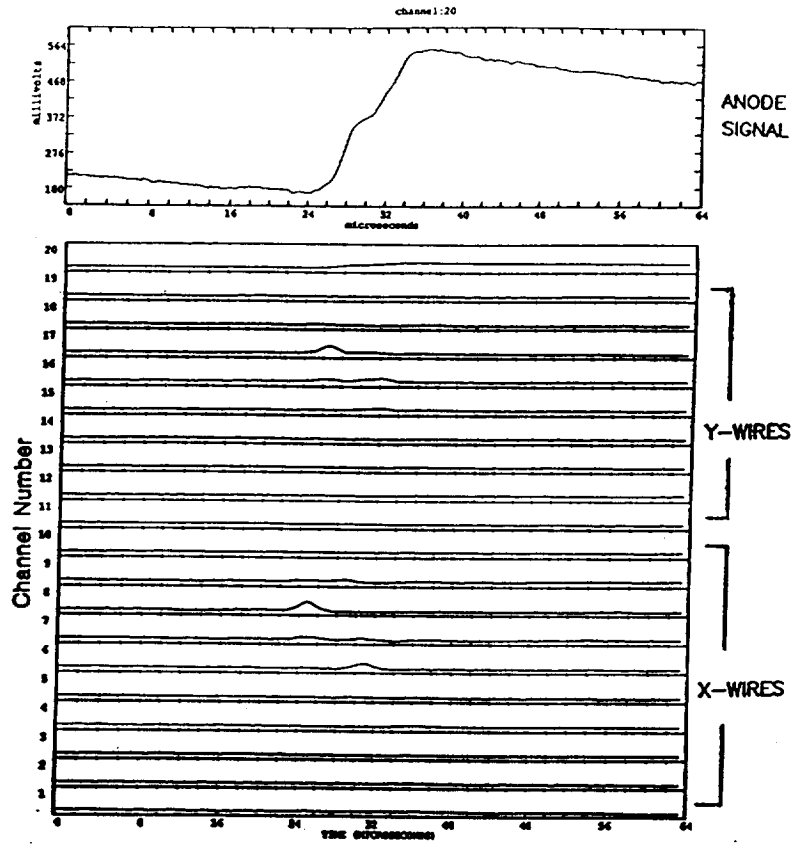

Fig. 16 On-line display of the digitized waveforms of the induction signals and anode signal for a γ-ray event

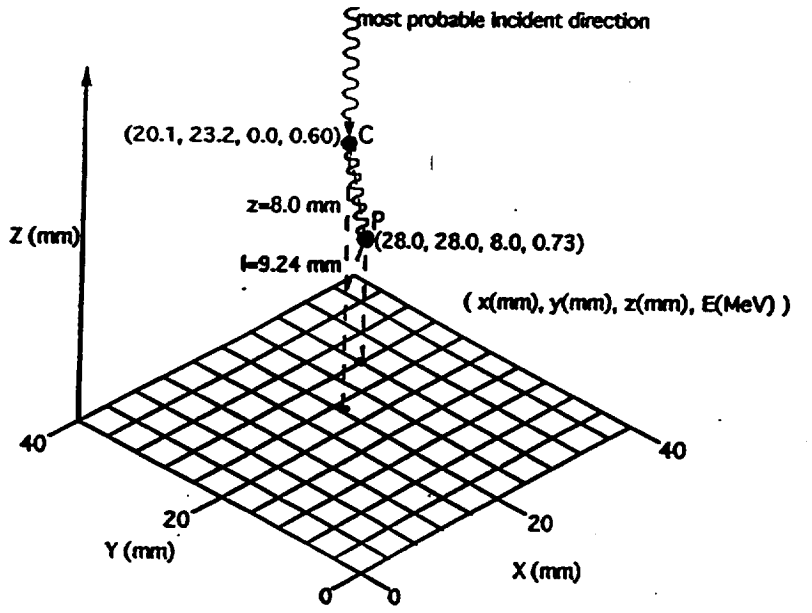

Fig. 17 An example of Compton scattered γ-ray event in the LXe

For the two-site event in Fig. 17, the function f has only one term

$$f = (W_0 - W_0')^2 = \left[\frac{0.511MeV * E_1}{E_2(1-\cos\theta_g)} - (E_1 + E_2)\right]^2$$

where, θ_g is the angle of the scattered photon relative to the vertical direction, obtained from geometry measurement. The correct interaction order and hence the first Compton interaction point are identified by the energy assignment which gives the smaller f value. $f = 0.23$ if $E_1 = 0.73$ MeV, but $f = 0.01$ if $E_1 = 0.60$ MeV. Blob A is the first interaction point.

We have shown that the intrinsic imaging capability of the LXe-TPC provides the energy and spatial information for each interaction point of a γ-ray within the sensitive volume. As a result, Compton kinematics enables the reconstruction of the direction of the incoming γ-ray, and a LXe-TPC can work as a Compton telescope, as discussed in the original paper[2]. However, the resulting angular resolution for the MeV region is limited by the small separation between two successive γ-ray interactions in the dense LXe. While not sufficient for source imaging, this limited angular resolution is however good enough for event identification and background rejection.

In a Compton telescope, the incident γ-ray direction lies on the surface of a cone, of half angle θ_c, and the cone's axis is given by the direction of the scattered γ-ray. The cone opening angle is calculated from the measured energy deposition at different interaction points using the Compton kinematics, as previous shown. The projection of this cone onto the celestial sphere is called the event circle. The center of the circle is determined by the direction of the scattered γ-ray, and the event circle radius is identical to the derived Compton scattering angle. A γ-ray point source is then located as the intersection point of all the individual event circles of fully absorbed γ-rays.

Fig. 18 illustrates the event circles for 22 γ-rays which were recorded with a ^{22}Na point source placed 40 cm above the sensitive area. To accept only γ-rays within 1° solid angle, and thus approach a parallel flux situation, we covered the sensitive area by a lead block with a 1 cm diameter hole. To improve signal/noise only events with two interaction points were selected. The Compton imaging capability of this LXe-TPC is obvious. Any event with event circle outside the FOV can be identified and considered as background event. As we have shown, the event reconstruction based on Compton kinematics does not require the absolute drift time as referred to the time zero provided by the light trigger. However, the absolute Z coordinate of an interaction point is necessary to reject low energy background events by fiducial volume cuts[5]. Withqut light trigger, as in the case of a doped LXe detector, this information can still be obtained from the prompt grid signal. Fig. 19 shows for example the grid and anode signal as recorded for a γ-ray event in our TPC. The starting time of the grid signal directly gives the Z location of the interaction point.

4. CONCLUSIONS AND PERSPECTIVE

A new type of γ-ray telescope has been proposed to image the MeV γ-ray flux from galactic and extragalactic sources, with high efficiency, good energy resolution, low background and arcminute localization accuracy. The telescope is based on a LXe-TPC as 3-D position sensitive detector and spectrometer, coupled to a coded aperture mask.

To demonstrate the feasibility of an imaging liquid xenon detector, a 10 liter LXe-TPC prototype has been built and tested. The required ppb purity level for the liquid has been achieved with a simple purification system. We have checked that the spectral and imaging performance of this LXe-TPC system is stable and reliable. Despite the much larger volume and much longer drift distance, the noise-subtracted energy resolution measured with this prototype is comparable, at the same electric field of 1 and 2 kV/cm, to that previously measured with simple ionization chambers.

We have also demonstrated the 3-D imaging capability with a novel non-destructive readout structure. The application of Compton event reconstruction for background identification and rejection has been tested.

Improvement of the energy resolution performance of this imaging detector will be achievd by using TMA doped LXe.

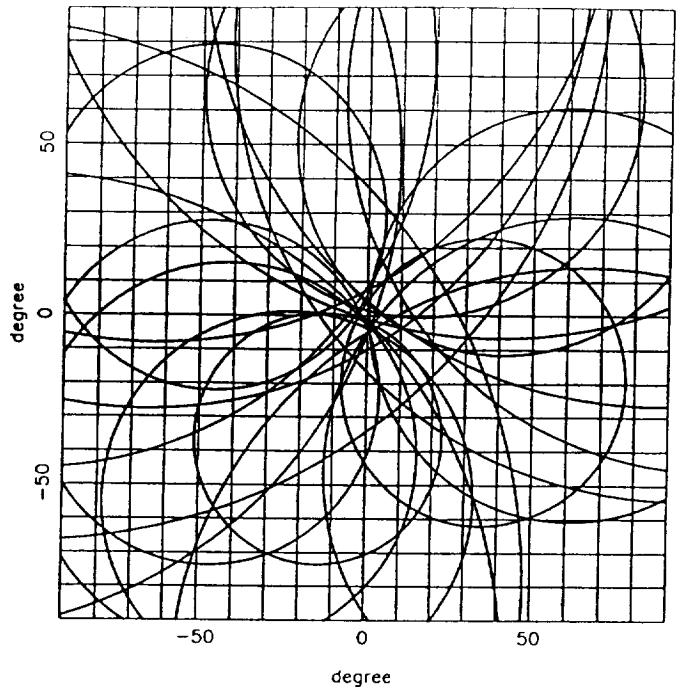

Fig. 18 Reconstruction of the "event circles" for 22 ^{22}Na γ-ray events from a point source

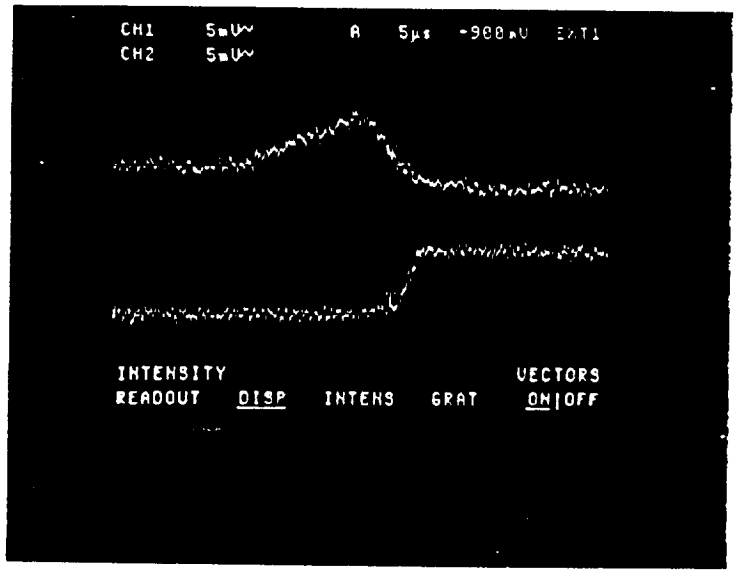

Fig. 19 Grid and Anode signal for a ^{22}Na γ-ray interaction in the LXe-TPC. The time scale is 5 µs/div.

Improvement on the spatial resolution will be achieved by improving the performance of the electronics and by reducing the wire spacing to 2 mm.

The ultimate spatial resolution limit, both for the Z and the $X - Y$ information, is set by diffusion and the finite extension of the charge blob in LXe, which is on the order of 0.5 mm for a 1 MeV electron.

5. ACKNOWLEDGMENTS

This work was supported by NASA grant NAGW-2013. We would like to thank our collaborators from Waseda University, the University of New Hampshire and Marshall Space Flight Center for their contribution and support. We are especially indebted with T. Doke, J. Kikuchi, T. Kashiwagi, K. Masuda and T. Fujino for their scientific, technical and financial support throughout the development of the 10 liter prototype. We would also like to acknowledge and thank the contribution of many colleagues, and in particular D. Schinzel, P. Picchi, A. Pepato, T. Lindblad and M. Minerskjold.

6. REFERENCES

[1] E. Aprile et al., "Determination of the ^{26}Al Celestial Source Distribution," in preparation for Ap.J. (Aug. 94)
[2] E. Aprile et al. SPIE Conf. Proc. 1159(1989) p.295
[3] E. Aprile et al., "A High Resolution Liquid Xenon Imaging Telescope for 0.3 - 10 MeV Gamma-Ray Astrophysics: Construction and Initial Balloon Flights," NASA proposal, CAL-2015 (1992).
[4] E. E. Fenimore and T.M. Cannon, Apple. Opt. 17 (1978) 337
[5] E. Aprile, A. Bolotnikov, D. Chen and R. Mukherjee, Nucl. Instr. and Meth. A327 (1993) 216.
[6] E. Aprile et al., Ap.J. Supplement Series, 92(1994)689
[7] E. Aprile, R. Mukherjee and M. Suzuki, Nucl. Instr. and Meth. A300 (1991) 343.
[8] E. Aprile, et at., IEEE Trans. Nucl. Sci., NS-37, No. 2, 553
[9] E. Aprile, R. Mukherjee and M. Suzuki, Nucl. Instr. and Meth. A302 (1991) 177.
[10] E. Aprile et al., Nucl. Instr. and Meth. A316 (1992) 29.
[11] E. Aprile, A. Bolotnikov, D. Chen and R. Mukherjee, SPIE Vol. 1734, Gamma-Ray Detectors (1992) 98.
[12] Oxisorb is a trade mark of Messer Griesheim GmbH.
[13] E. Shibamura et al., Phys. Rev. A 20 (1979) 2547.
[14] O. Bunemann, T.E. Cranshaw, and I.A. Harvey, Can. J. of Res., 27 (1947) 191.
[15] H. Ichinose et al., Nucl. Instr. and Meth. A322 (1992) 216.
[16] E. Aprile et al., "Performance of a 3.5 liter LXe TPC triggered by the scintillation light as γ-ray detector", in preparation for NIM, (Sept. 1994)
[17] A. Galper et al., Pribory i Teknika Eksperimenta, 1(1981)649